



Differential involvement of LUBAC-mediated linear ubiquitination in intestinal epithelial cells and macrophages during intestinal inflammation

Journal:	<i>The Journal of Pathology</i>
Manuscript ID	JPATH-2022-369.R1
Wiley - Manuscript type:	Original Article
Date Submitted by the Author:	n/a
Complete List of Authors:	<p>Sakamoto, Yusuke; Kyoto Daigaku Daigakuin Igaku Kenkyuka Igakubu, Department of Surgery</p> <p>Sasaki, Katsuhiro; Kyoto Daigaku Daigakuin Igaku Kenkyuka Igakubu, Molecular and Cellular Physiology</p> <p>Omatsu, Mayuki; Kyoto University Graduate School of Medicine Department of Gastroenterology and Hepatology, Department of Gastroenterology and Hepatology</p> <p>Hamada, Kensuke; Kyoto University Graduate School of Medicine Department of Gastroenterology and Hepatology, Department of Gastroenterology and Hepatology</p> <p>Nakanishi, Yuki; Kyoto University Graduate School of Medicine Department of Gastroenterology and Hepatology, Department of Gastroenterology & Hepatology;</p> <p>Itatani, Yoshiro ; Kyoto Daigaku Daigakuin Igaku Kenkyuka Igakubu, Department of Surgery</p> <p>Kawada, Kenji; Kyoto University Graduate School of Medicine, Surgery</p> <p>Obama, Kazutaka; Kyoto University Graduate School of Medicine, Surgery</p> <p>Seno, Hiroshi; Kyoto University Graduate School of Medicine, Department of Gastroenterology and Hepatology</p> <p>Iwai, Kazuhiro; Kyoto Daigaku Daigakuin Igaku Kenkyuka Igakubu, Molecular and Cellular Physiology</p>
Portal Keywords:	Colon, Chronic inflammation, In vivo models, Knock-out models, Apoptosis
Tissue:	
Pathology:	
Technique:	

SCHOLARONE™
Manuscripts

1
2
3
4
5
6
7
8
9
10
11
12
13
14
15
16
17
18
19
20
21
22
23
24
25
26
27
28
29
30
31
32
33
34
35
36
37
38
39
40
41
42
43
44
45
46
47
48
49
50
51
52
53
54
55
56
57
58
59
60

1
2
3 **Article manuscript (Main text 3,989 words)**
4

5 **2 Title**
6

7 **3 Differential involvement of LUBAC-mediated linear ubiquitination in intestinal epithelial**
8 **4 cells and macrophages during intestinal inflammation**
9

10 **5**
11
12 **6 Running title (68 characters)**
13

14
15
16
17 Linear ubiquitination in intestinal epithelial cells and macrophages
18

19
20
21 **9 Authors and affiliations**
22

23
24 **10 Yusuke Sakamoto^{1,2}, Katsuhiko Sasaki¹, Mayuki Omatsu³, Kensuke Hamada³, Yuki**
25
26 **11 Nakanishi³, Yoshiro Itatani², Kenji Kawada², Kazutaka Obama², Hiroshi Seno³ and**
27
28 **12 Kazuhiro Iwai^{1*}**
29

30
31
32
33 ¹Department of Molecular and Cellular Physiology, Graduate School of Medicine, Kyoto
34
35 University, Kyoto, Japan.
36

37 ²Department of Surgery, Graduate School of Medicine, Kyoto University, Kyoto, Japan.
38

39
40 ³Department of Gastroenterology and Hepatology, Graduate School of Medicine, Kyoto
41
42 University, Kyoto, Japan.
43

44
45
46 **20 *Correspondence to**
47

48
49 Kazuhiro Iwai
50

51
52 Department of Molecular and Cellular Physiology, Graduate School of Medicine, Kyoto
53
54 University, Yoshida-Konoe-cho, Sakyo-ku, Kyoto 606-8501, Japan
55

56
57 Phone: +81-75-753-4671; Fax: +81-75-753-4676
58

59
60 E-mail: kiwai@mcp.med.kyoto-u.ac.jp

1
2
3
4
5
6
7
8
9
10
11
12
13
14
15
16
17
18
19
20
21
22
23
24
25
26
27
28
29
30
31
32
33
34
35
36
37
38
39
40
41
42
43
44
45
46
47
48
49
50
51
52
53
54
55
56
57
58
59
60

26

27 **Conflict of interest statement**

28 The authors declare no competing financial interests.

For Peer Review

1
2
3 **29 Abstract (284 words)**
4

5 **30 Disruption of the intestinal epithelial barrier and dysregulation of macrophages are**
6
7 **31 major factors contributing to the pathogenesis of inflammatory bowel diseases (IBDs).**
8
9 **32 Activation of NF- κ B and cell death are involved in maintaining intestinal homeostasis in**
10
11 **33 a cell type-dependent manner. Although both are regulated by linear ubiquitin chain**
12
13 **34 assembly complex (LUBAC)-mediated linear ubiquitination, the physiological relevance**
14
15 **35 of linear ubiquitination to intestinal inflammation remains unexplored. Here, we used two**
16
17 **36 experimental mouse models of IBD (intraperitoneal LPS and oral dextran sodium**
18
19 **37 sulphate (DSS) administration) to examine the role of linear ubiquitination in intestinal**
20
21 **38 epithelial cells (IECs) and macrophages during intestinal inflammation. We did this by**
22
23 **39 deleting the linear ubiquitination activity of LUBAC specifically from IECs or**
24
25 **40 macrophages. Upon LPS administration, loss of ligase activity in IECs induced mucosal**
26
27 **41 inflammation and augmented IEC death. LPS-mediated death of LUBAC-defective IECs**
28
29 **42 was triggered by TNF. IEC death was rescued by an anti-TNF antibody, and TNF (but**
30
31 **43 not LPS) induced apoptosis of organoids derived from LUBAC-defective IECs. However,**
32
33 **44 augmented TNF-mediated IEC death did not overtly affect the severity of colitis after DSS**
34
35 **45 administration. By contrast, defective LUBAC ligase activity in macrophages ameliorated**
36
37 **46 DSS-induced colitis by attenuating both infiltration of macrophages and expression of**
38
39 **47 inflammatory cytokines. Decreased production of macrophage chemoattractant MCP-**
40
41 **48 1/CCL2, as well as pro-inflammatory IL-6 and TNF, occurred through impaired**
42
43 **49 activation of NF- κ B and ERK via loss of ligase activity in macrophages. Taken together,**
44
45 **50 these results indicate that both intraperitoneal LPS and oral DSS administrations are**
46
47 **51 beneficial for evaluating epithelial integrity under inflammatory conditions, as well as**
48
49 **52 macrophage functions in the event of an epithelial barrier breach. The data clarify the**
50
51 **53 cell-specific roles of linear ubiquitination as a critical regulator of TNF-mediated**
52
53
54
55
56
57
58
59
60

1
2
3
4
5
6
7
8
9
10
11
12
13
14
15
16
17
18
19
20
21
22
23
24
25
26
27
28
29
30
31
32
33
34
35
36
37
38
39
40
41
42
43
44
45
46
47
48
49
50
51
52
53
54
55
56
57
58
59
60

**54 epithelial integrity and macrophage pro-inflammatory responses during intestinal
55 inflammation.**

56

57 Keywords (10)

58 LUBAC; linear ubiquitination; NF- κ B; cell death; intestinal epithelial cells;

59 macrophages; DSS; LPS; IBD; intestinal inflammation

For Peer Review

60 Introduction

61 Inflammatory bowel diseases (IBDs), including Crohn's disease and ulcerative colitis, are
62 characterized by chronic and relapsing inflammation in the gut; these conditions affect 6.8
63 million individuals worldwide [1]. Although the pathogenesis of IBDs is thought to involve
64 genetic, environmental, microbial, epithelial, and immune factors, the pathophysiology still
65 remains unclear, resulting in inadequate responses to currently available treatments [2-4].
66 Recent studies show that the innate immune system, including epithelial barrier function and
67 microbial sensing by macrophages, also plays an important role in the pathogenesis of IBDs,
68 as do adaptive immune responses such as T cell-derived inflammatory cytokines [5-7].

69 Intestinal epithelial cells (IECs) maintain intestinal homeostasis by forming a physical and
70 chemical barrier that protects intestinal tissue from invading intraluminal bacteria [8-10]. IEC
71 death disrupts intestinal homeostasis in some mouse models [11-18], and excessive IEC death
72 is observed in patients with IBDs [19, 20]. In addition, macrophages, major components of the
73 innate immune system that reside just beneath IECs, play crucial roles as the first line of defense
74 [21-24]. When intestinal homeostasis is perturbed by genetic or environmental factors such as
75 epithelial barrier disruption or macrophage dysregulation, a large number of TLR-expressing
76 pro-inflammatory macrophages migrate into the inflamed mucosa and release pro-
77 inflammatory cytokines and chemokines such as IL-6, TNF, and MCP-1/CCL2 [22-24] in
78 response to products derived from invading bacteria [25]. Although appropriate responses
79 confer protection against bacteria and promote tissue regeneration by acting on other immune
80 cells and IECs, uncontrolled responses lead to persistent inflammation, which inhibits tissue
81 repair [22-24, 26-28].

82 The linear ubiquitin chain assembly complex (LUBAC), comprising HOIP, HOIL-1L, and
83 SHARPIN, activates the NF- κ B signaling pathway and inhibits programmed cell death by
84 generating unique N-terminal-linked linear polyubiquitin chains via the catalytic center in

1
2
3 85 HOIP [29-32]. Several reports suggest that NF- κ B activation maintains IEC homeostasis by
4
5 86 inhibiting IEC death; however, activation of NF- κ B in macrophages plays a pro-inflammatory
6
7
8 87 role [33-36]. Recent genome-wide association studies also show that NF- κ B is associated with
9
10
11 88 IBDs [37]. Despite the essential roles played by NF- κ B and cell death during intestinal
12
13 89 inflammation, involvement of LUBAC-mediated linear ubiquitination is unclear.

14
15 90 Considering the cell type-specific roles of both NF- κ B and cell death [33, 38], we used mice
16
17 91 lacking the C-terminal catalytic center of HOIP specifically in IECs (HOIP^{IEC- Δ lin}) or
18
19 92 macrophages (HOIP^{MYE- Δ lin}) to examine the role of linear ubiquitination in IECs and
20
21 93 macrophages. Since no spontaneous intestinal phenotype was observed in either mouse model,
22
23 94 we used mouse models of IBD generated by intraperitoneal administration of LPS or by oral
24
25 95 administration of dextran sodium sulphate (DSS) [39, 40]. Loss of ligase activity in IECs
26
27 96 provoked mucosal inflammation and augmented TNF-mediated IEC death upon LPS
28
29 97 administration, indicating that linear ubiquitination in IECs protects against intestinal
30
31 98 inflammation and suppresses TNF-induced IEC death under inflammatory conditions. By
32
33 99 contrast, loss of LUBAC ligase activity in macrophages alleviated DSS-induced colitis and
34
35 100 impaired NF- κ B- and ERK-mediated inflammatory cytokine production upon TLR stimulation,
36
37 101 indicating that linear ubiquitination in macrophages augments intestinal inflammation in the
38
39 102 event of an epithelial barrier breach. These findings demonstrate that linear ubiquitination in
40
41 103 IECs and macrophages plays differential roles to maintain both TNF-mediated epithelial
42
43 104 integrity and macrophage pro-inflammatory responses to regulate intestinal inflammation.
44
45
46
47
48
49
50
51
52
53
54
55
56
57
58
59
60

105 **Materials and methods**

106 Mice

107 HOIP^{Δlin-flox/Δlin-flox} mice, in which the C-terminal catalytic center of HOIP (*Rnf31*) is flanked
108 by two *loxP* sites, have been described previously [41, 42]. HOIP^{Δlin-flox/Δlin-flox} mice were
109 crossed with *Villin-Cre* [43] or *LysM-Cre* [44] mice to ablate the ligase activity of HOIP in
110 IECs or macrophages, respectively. Unless specified otherwise, mice (aged 8 to 12 weeks) were
111 cohoused with sex-matched littermates under specific pathogen-free conditions. All animal
112 protocols were approved by Kyoto University.

114 Antibodies

115 The antibodies used in this study are listed in Supplementary materials and methods.

117 LPS and TNF-induced IEC death

118 Mice were injected intraperitoneally with LPS (10 μg/g bodyweight (BW), *Escherichia coli*
119 055:B5; Sigma-Aldrich, St. Louis, MO, USA) or recombinant mouse TNF-α (0.1 μg/g BW;
120 R&D Systems, Minneapolis, MN, USA).

122 TNF depletion experiments

123 Mice were injected intraperitoneally with an anti-TNF-α antibody (200 μg, clone XT3.11; Bio
124 X Cell, Lebanon, NH, USA) or an isotype control IgG (200 μg, clone TNP6A7; Bio X Cell) 1
125 h before LPS challenge.

127 Induction of colitis

128 Experimental colitis was induced by oral administration of 2.0% or 1.5% DSS (MP Biomedicals,
129 Irvine, CA, USA) dissolved in drinking water (ingested for 7 or 5 days), followed by of normal

1
2
3 130 water (ingested for 2 or 5 days).
4

5 131

6
7
8 132 Histological analysis

9
10 133 The distal third of the colon or ileal segment was fixed in 10% formalin and embedded in
11
12 134 paraffin. The severity of DSS-induced colitis was determined by examining H&E-stained
13
14 135 sections, as described previously [45]. Multiple viewing fields per slide were acquired
15
16 136 randomly under an Olympus BX51 upright microscope (Olympus, Tokyo, Japan) or a
17
18 137 FLUOVIEW FV1000 confocal laser scanning microscope (Olympus).
19
20

21 138

22
23
24 139 IEC isolation and organoid culture

25
26 140 IEC isolation and generation of organoids were performed as previously described [46]. To
27
28 141 examine cell death, cells were stained with 5 μ M SYTOX Green nucleic acid stain (Invitrogen,
29
30 142 Waltham, MA, USA) and 5 μ g/ml Hoechst 33342 nucleic acid stain (Invitrogen), which were
31
32 143 added to the medium, followed by observation under an IX83 Inverted Research Microscope
33
34 144 (Olympus). Organoids were treated with LPS (Sigma-Aldrich) or TNF- α (R&D Systems). Z-
35
36 145 VAD-FMK (ZVAD) (PEPTIDE, Osaka, Japan) was added 1 h before TNF treatment.
37
38
39

40 146

41
42
43 147 Enrichment of bone marrow-derived macrophages

44
45 148 Bone marrow-derived macrophages (BMDMs) were isolated from bone marrow from the tibia
46
47 149 and femur and cultured for 7 days in complete RPMI containing 20 ng/ml recombinant murine
48
49 150 M-CSF (BioLegend, San Diego, CA, USA). BMDMs were stimulated with TNF, LPS,
50
51 151 Poly(I:C) (InvivoGen, San Diego, CA, USA), CpG-B (InvivoGen), or Pam3CSK4 (InvivoGen).
52
53 152 For some experiments, HOIPin-8 (Axon Medchem LLC, Reston, VA, USA) or a MEK inhibitor
54
55 153 (PD0325901; FUJIFILM, Osaka, Japan) was added before stimulation.
56
57
58

59 154
60

1
2
3 155 Statistical analysis
4

5 156 Results are expressed as the mean \pm SEM. Statistical analyses were performed using

7 157 GraphPad Prism Version9.3.1 (GraphPad Software, San Diego, CA, USA). All statistical tests

9
10 158 are indicated in each figure legend. The significance level was set at $P < 0.05$.
11

12 159
13
14
15
16
17
18
19
20
21
22
23
24
25
26
27
28
29
30
31
32
33
34
35
36
37
38
39
40
41
42
43
44
45
46
47
48
49
50
51
52
53
54
55
56
57
58
59
60

For Peer Review

160 Results

161 Mice lacking linear ubiquitination activity in IECs display mucosal inflammation and 162 augmented IEC death upon intraperitoneal administration of LPS

163 To investigate the role of LUBAC-mediated linear ubiquitination in IECs, we crossed
164 HOIP^{Δlin-flox/Δlin-flox} mice [41, 42] with *Villin-Cre* mice [43] to delete the linear ubiquitination
165 activity of LUBAC (HOIP^{Δlinear}) specifically in IECs (HOIP^{IEC-Δlin} mice) (supplementary
166 material, Figure S1A). Immunoblotting revealed that *Cre*-mediated recombination of HOIP loci
167 (*Rnf31*), as evaluated by the decrease in full-length HOIP, was not complete (expression of full-
168 length HOIP in the colon and the small intestine of HOIP^{IEC-Δlin} mice was 49.2 ± 2.1% and 28.8
169 ± 3.7%, respectively, of that observed in control HOIP^{Δlin-flox/Δlin-flox} mice; supplementary
170 material, Figure S1B). This was also the case for organoid cultures (31.5 ± 5.4% expression in
171 HOIP^{IEC-Δlin} organoids compared with control organoids; supplementary material, Figure S1B).
172 The amounts of HOIL-1L and SHARPIN, the other two subunits of LUBAC, were also reduced
173 (supplementary material, Figure S1B). HOIP^{IEC-Δlin} mice developed normally (supplementary
174 material, Figure S1C); however, whole-body deletion of HOIP was embryonic lethal [47, 48].
175 There were no overt changes in tissue architecture, nor defects in IEC differentiation, in the
176 colon or small intestine under steady-state conditions (supplementary material, Figure S1D–F).

177 Intraperitoneal administration of LPS causes shedding of IECs in the small intestine
178 [39, 49]. LUBAC-mediated linear ubiquitination plays a role in protecting cells from
179 programmed cell death [30, 32, 50, 51]. We found that HOIP^{IEC-Δlin} mice were extremely
180 sensitive to intraperitoneal administration of LPS; these mice showed a significant reduction in
181 colon length, and marked mucosal damage in the distal colon, at 24 h post-LPS treatment
182 (Figure 1A, B). Immunohistological analysis revealed increased infiltration of the distal colon
183 by leukocytes, including macrophages (Figure 1C, D and supplementary material, Figure S2).
184 Moreover, at 4 h post-LPS administration the number of apoptotic cells that were cleaved

1
2
3 185 caspase 3- and TUNEL-positive was higher in the distal colon of HOIP^{IEC-Δlin} mice than in that
4
5 186 of control mice, although there was no difference in the number of apoptotic cells under steady-
6
7 187 state conditions (Figure 1E, F). In particular, apoptotic cells were detected in all layers of the
8
9 188 distal colon, including the crypt bottom, in HOIP^{IEC-Δlin} mice (Figure 1E, F). The inflammatory
10
11 189 changes in the distal colon in HOIP^{IEC-Δlin} mice were not observed in the small intestine
12
13 190 (supplementary material, Figure S3A). However, apoptotic cells were detected in the crypts and
14
15 191 villous tips in HOIP^{IEC-Δlin} small intestine at 1.5 h post-LPS administration, along with an
16
17 192 increase in the number of apoptotic IECs; however, apoptotic cells were observed only at the
18
19 193 villous tips in the small intestine of control mice, regardless of LPS administration
20
21 194 (supplementary material, Figure S3B, C) [39, 52]. Taken together, these data suggest that loss
22
23 195 of LUBAC ligase activity in IECs renders mice more sensitive to IEC death in the colon and
24
25 196 small intestine after intraperitoneal injection of LPS, which may lead to mucosal inflammation
26
27 197 (although no inflammatory changes were observed in the small intestine).
28
29
30
31
32
33
34
35

199 **TNF drives LPS-induced mucosal inflammation and augmented IEC death in mice** 200 **lacking epithelial LUBAC ligase activity**

201 To examine the mechanism underlying IEC death in LPS-treated HOIP^{IEC-Δlin} mice,
202 we established intestinal epithelial organoids. There were no morphological differences
203 between HOIP^{IEC-Δlin} and control organoids, and LPS-treatments induced no apparent
204 morphological changes in the organoids (Figure 2A). Because shedding of IECs is thought to
205 be triggered by inflammatory cytokines produced by LPS-stimulated macrophages [39, 49],
206 and LUBAC-mediated linear ubiquitination protects cells from TNF-induced cell death
207 (including apoptosis and necroptosis) [30, 32, 50, 51], we focused on TNF as LPS
208 administration induced expression of TNF in the serum and colon tissues of HOIP^{IEC-Δlin} and
209 control mice (Figure 2B, C). We found that HOIP^{IEC-Δlin} organoids exhibited a disrupted and

1
2
3 210 dark appearance as early as 24 h after TNF treatment (Figure 2A). After treatment with TNF,
4
5 211 the proportion of SYTOX Green-positive organoids was higher for HOIP^{IEC-Δlin} than for
6
7
8 212 controls, indicating that TNF, but not LPS, is responsible for cell death in HOIP^{IEC-Δlin} organoids
9
10 213 (Figure 2A). Immunoblotting revealed that cleavage of both caspase 8 and 3 was higher in TNF-
11
12 214 treated HOIP^{IEC-Δlin} organoids, whereas phosphorylation of MLKL, an executor of necroptosis,
13
14 215 was not detected in either HOIP^{IEC-Δlin} or control organoids (Figure 2D). These data suggest that
15
16 216 TNF preferentially triggers apoptosis of HOIP^{IEC-Δlin} organoids. In addition, degradation of
17
18 217 IκBα, a hallmark of NF-κB activation, was impaired substantially in HOIP^{IEC-Δlin} organoids
19
20 218 upon TNF stimulation (Figure 2E), and expression of NF-κB target genes, including anti-
21
22 219 apoptotic genes, was partially attenuated in HOIP^{IEC-Δlin} organoids exposed to TNF (Figure 2F).
23
24 220 These results indicate that loss of LUBAC ligase activity sensitizes organoids to TNF-induced
25
26 221 apoptosis (at least in part) by impairing NF-κB activation.
27
28
29
30
31

32 222 Intraperitoneal injections of TNF provoked mucosal inflammation in the colon of
33
34 223 HOIP^{IEC-Δlin} mice, with shortening of the colon and increased invasion by inflammatory cells;
35
36 224 this was not observed in control mice (Figure 3A–D and supplementary material, Figure S2).
37
38 225 Immunohistochemical analysis revealed increased numbers of cleaved caspase 3-positive IECs
39
40 226 in the colon of HOIP^{IEC-Δlin} mice (Figure 3E). Although H&E staining revealed that changes in
41
42 227 the small intestine of HOIP^{IEC-Δlin} mice were less pronounced than those in the colon
43
44 228 (supplementary material, Figure S3D), cleaved caspase 3-positive apoptotic cells in the small
45
46 229 intestine of TNF-treated HOIP^{IEC-Δlin} mice were observed at the crypt bottom and the villous
47
48 230 tips (supplementary material, Figure S3E, F). Pretreatment with the anti-TNF antibody
49
50 231 prevented LPS-induced inflammatory changes in HOIP^{IEC-Δlin} mice, including shortening of the
51
52 232 colon, infiltration of the colon by immune cells and apoptosis of IECs (Figure 3F–J and
53
54 233 supplementary material, Figure S3G–I). Collectively, these results indicate that LUBAC-
55
56
57
58
59
60

1
2
3 234 induced linear ubiquitination protects mice from LPS-induced mucosal inflammation and TNF-
4
5 235 induced IEC death.

6
7
8 236

9
10 237 **Defective LUBAC catalytic activity in macrophages, but not in IECs, ameliorates DSS-**
11
12 238 **induced colitis**

13
14 239 To examine whether IEC death in HOIP^{IEC-Δlin} mice has an effect on the phenotype
15
16 240 of another mouse model of IBD, we fed HOIP^{IEC-Δlin} and control mice with 2% or 1.5% DSS, a
17
18 241 direct chemical toxin to IECs [53], for 7 or 5 days. However, loss of the LUBAC ligase activity
19
20 242 in IECs did not overtly affect severity of DSS-induced colitis (including BW changes,
21
22 243 shortening of the colon, histological changes, or expression of inflammatory cytokines) (Figure
23
24 244 4A–D and supplementary material, Figure S4). In addition, we examined apoptotic IECs in
25
26 245 DSS-treated HOIP^{IEC-Δlin} mice, and observed cleaved caspase 3- and TUNEL-positive IECs in
27
28 246 some crypts that escaped DSS-induced direct injury (Figure 4E). Thus, we suspect that loss of
29
30 247 linear ubiquitination activity in IECs does not overtly affect the severity of DSS-induced colitis,
31
32 248 despite the tendency toward increased IEC death; this may be because DSS damages IECs
33
34 249 directly.

35
36 250 Next, we examined the role played by linear ubiquitination in macrophages during
37
38 251 intestinal inflammation because macrophages represent the first line of defense after epithelial
39
40 252 barrier disruption [24]. To this end, we crossed HOIP^{Δlin-flox/Δlin-flox} mice with *LysM-Cre* mice
41
42 253 [44] to generate mice lacking the catalytic center of HOIP specifically in macrophages
43
44 254 (HOIP^{MYE-Δlin}). We observed a marked reduction ($44.2 \pm 0.7\%$) in expression of full-length
45
46 255 HOIP, along with HOIL-1L and SHARPIN, in HOIP^{MYE-Δlin} BMDMs compared with control
47
48 256 BMDMs (supplementary material, Figure S5A, B). This was also the case for peritoneal
49
50 257 macrophages, in which expression of full-length HOIP in HOIP^{MYE-Δlin} mice was attenuated
51
52 258 significantly, albeit not completely (supplementary material, Figure S5A). HOIP^{MYE-Δlin} mice

1
2
3 259 developed normally, and no inflammatory or autoimmune phenotypes were observed in the
4
5 260 intestine or the skin of aged HOIP^{MYE-Δlin} mice (supplementary material, Figure S5C, D).
6
7
8 261 Additionally, there was no abnormality in the proportions of activated lymphocytes, including
9
10 262 germinal center B cells (PNA⁺FAS⁺), activated T cells (CD25⁺CD69⁺), or effector T cells
11
12 263 (CD44^{hi}CD62L^{lo}), in the spleen or peripheral lymph nodes of aged HOIP^{MYE-Δlin} mice
13
14
15 264 (supplementary material, Figure S6).

16
17 265 To evaluate involvement of linear ubiquitination in macrophages after an epithelial
18
19 266 barrier breach, we fed HOIP^{MYE-Δlin} and control mice with DSS. We found that inflammatory
20
21 267 changes, including weight loss and shortening of the colon, were less severe in HOIP^{MYE-Δlin}
22
23 268 mice than in control mice (Figure 5A, B). Histological analysis revealed that mucosal damage
24
25 269 in the distal colon was less severe in HOIP^{MYE-Δlin} mice than in control mice (Figure 5C).
26
27 270 Immunohistological analysis also showed that the number of the leukocytes, including
28
29 271 macrophages, B cells, and T cells, was lower in DSS-treated HOIP^{MYE-Δlin} mice (Figure 5D, E
30
31 272 and supplementary material, Figure S7). Moreover, expression of inflammatory cytokines in
32
33 273 the colon was significantly lower (Figure 5F). Next, we injected HOIP^{MYE-Δlin} and control mice
34
35 274 intraperitoneally with LPS, because macrophages are thought to be involved in the pathogenesis
36
37 275 of the LPS-induced IEC shedding [39]. However, regardless of LUBAC ligase activity, we
38
39 276 found no overt differences in the number of apoptotic IECs in the small intestine, or the levels
40
41 277 of inflammatory cytokines in serum or intestinal tissue (supplementary material, Figure S8).
42
43 278 Collectively, the data suggest that attenuated linear ubiquitination in macrophages ameliorates
44
45 279 the severity of colitis after an epithelial breach induced by DSS.
46
47
48
49
50
51

52 280

53
54
55 281 **Attenuation of LUBAC ligase activity in macrophages impairs NF-κB- and ERK-**
56
57 282 **mediated production of inflammatory cytokines in response to TLR stimulation**
58
59
60

1
2
3 283 To address the molecular mechanisms underlying amelioration of DSS-induced
4
5 284 colitis in HOIP^{MYE-Δlin} mice, we stimulated BMDMs from HOIP^{MYE-Δlin} and control mice with
6
7
8 285 TNF [30-32]. We found that phosphorylation and degradation of IκBα, as well as
9
10 286 phosphorylation of p65 and IKK, were lower in TNF-stimulated HOIP^{MYE-Δlin} BMDMs than in
11
12 287 control BMDMs (Figure 6A). Studies suggest that TLRs expressed by pro-inflammatory
13
14 288 macrophages play a role in DSS-induced colitis [22, 23]. Upon LPS stimulation, not only
15
16 289 phosphorylation and degradation of IκBα, but also phosphorylation of IKK and p65, was
17
18 290 impaired in HOIP^{MYE-Δlin} BMDMs (Figure 6B), indicating that loss of LUBAC ligase activity
19
20 291 in macrophages attenuates LPS-mediated activation of NF-κB. IKK activation in macrophages
21
22 292 leads to activation of ERK [42, 54, 55]; here, we found that LPS-induced phosphorylation of
23
24 293 ERK was lower in HOIP^{MYE-Δlin} BMDMs than in control BMDMs (Figure 6C). By contrast,
25
26 294 loss of LUBAC ligase activity did not overtly affect activation of other MAPK pathways,
27
28 295 including p38 and JNK (Figure 6C). To confirm the role of LUBAC-mediated linear
29
30 296 ubiquitination during LPS signaling in macrophages, we treated BMDMs from WT mice with
31
32 297 HOIPin-8, a specific inhibitor of LUBAC ligase activity [56]. As shown in Figure 6D, LPS-
33
34 298 mediated activation of NF-κB and ERK was attenuated markedly by HOIPin-8, whereas
35
36 299 activation of JNK and p38 was not. These results indicate that linear ubiquitination is involved
37
38 300 in LPS-triggered activation of NF-κB and ERK, but not p38 or JNK, in macrophages.
39
40 301 Augmented cell death is observed in some cells with attenuated LUBAC activity [30, 32, 50,
41
42 302 51]. However, linear ubiquitination in macrophages has no obvious effect on TNF-mediated
43
44 303 cell death, regardless of the presence of cycloheximide, or LPS-induced cell death in HOIP<sup>MYE-
45
46 304 Δlin</sup> BMDMs, or DSS-treated HOIP^{MYE-Δlin} mice (supplementary material, Figure S9).

47
48 305 Next, we asked how loss of linear ubiquitination affects inflammatory cytokine
49
50 306 production upon TLR stimulation. LPS-induced production of IL-6, TNF, and MCP-1/CCL2
51
52 307 (a chemoattractant for macrophages) fell significantly in HOIP^{MYE-Δlin} BMDMs and HOIPin-8-

1
2
3 308 treated BMDMs from WT mice (Figure 6E, F). Because treatment with a MEK inhibitor
4
5 309 suppressed TNF and MCP-1/CCL2 (Figure 6G), we speculated that ERK acts synergistically
6
7
8 310 with NF- κ B to trigger production of inflammatory cytokines. Lastly, we investigated LUBAC
9
10 311 involvement in other TLR signaling pathways. Upon stimulation with TLR ligands Poly(I:C),
11
12 312 CpG-B, or Pam3CSK4, phosphorylation and degradation of I κ B α , and phosphorylation of IKK
13
14
15 313 and p65, was substantially attenuated by pretreatment with HOIPin-8 (supplementary material,
16
17 314 Figure S10). ERK activation was impaired markedly by HOIPin-8 downstream of these ligands
18
19
20 315 (supplementary material, Figure S10). Furthermore, production of IL-6 by HOIP^{MYE- Δ lin}
21
22 316 BMDMs was impaired substantially in response to Poly(I:C), CpG-B, and Pam3CSK4 (Figure
23
24 317 6H), suggesting that linear ubiquitination is involved in signaling via multiple TLRs.
25
26
27 318 Collectively, these results suggest that linear ubiquitination in macrophages augments intestinal
28
29 319 inflammation in the event of an epithelial barrier breach induced by DSS, possibly due to
30
31 320 increased production of pro-inflammatory cytokines and a macrophage chemoattractant
32
33
34 321 downstream of NF- κ B and ERK pathway activation by multiple TLR ligands.
35
36
37
38
39
40
41
42
43
44
45
46
47
48
49
50
51
52
53
54
55
56
57
58
59
60

322 Discussion

323 Dysfunction of the epithelial barrier and unrestrained inflammatory responses by macrophages
324 are major factors contributing to the pathogenesis of IBDs [22-24, 57]. Since cell-specific
325 targeting is vital to uncover the roles of NF- κ B- and cell death-related pathways [33, 38], we
326 examined the role of LUBAC ligase activity, which controls NF- κ B activation and programmed
327 cell death [29-32], in both IECs and macrophages during intestinal inflammation. To do this,
328 we used two experimental mouse models of IBD. Loss of the LUBAC ligase activity in IECs
329 or macrophages resulted in different phenotypes: IEC-specific loss of linear ubiquitination
330 activity sensitized mice to mucosal inflammation after LPS administration, whereas loss of
331 activity in macrophages ameliorated DSS-induced colitis.

332 Mice with IEC-specific deletion of molecules essential for NF- κ B activation or protection
333 from TNF-mediated cell death exhibit spontaneous severe intestinal inflammation due to the
334 augmented sensitivity to TNF-induced cell death [11, 14]. However, HOIP^{IEC- Δ lin} mice did not
335 develop spontaneous histological abnormalities in the intestines (supplementary material,
336 Figure S1D-F), despite the crucial role of LUBAC-mediated linear ubiquitination in NF- κ B
337 activation and protection from cell death [32, 50, 51]. Observations in the intestines of HOIP^{IEC- Δ lin}
338 mice were in sharp contrast to those in skin (another border between the environment and
339 the body), in which attenuated LUBAC function triggers spontaneous dermatitis due to TNF-
340 mediated cell death [50, 58, 59]. The mechanisms responsible for the discrepancy between the
341 skin and intestine are unknown; however, the finding that LUBAC ligase activity in IECs is
342 dispensable for intestinal homeostasis enabled us to evaluate two IBD models: LPS-mediated
343 IEC shedding and DSS-induced colitis [39, 40]. Loss of the LUBAC ligase activity in IECs
344 rendered mice susceptible to mucosal inflammation and augmented IEC death upon
345 intraperitoneal injection of LPS (Figure 1); this was phenocopied by TNF injection (Figure 3A-
346 E), and was rescued by an anti-TNF antibody (Figure 3F-J). We also found that TNF induced

1
2
3 347 apoptosis of HOIP^{IEC-Δlin} organoids; however, LPS did not (Figure 2A, D), which was due in
4
5 348 part to the compromised NF-κB pathway (Figure 2E, F). At present, we do not know why we
6
7 349 could not detect inflammation in the small intestine of LPS-treated HOIP^{IEC-Δlin} mice, despite
8
9 350 augmented epithelial apoptosis (supplementary material, Figure S3A–C). However,
10
11 351 mechanisms other than NF-κB- or LUBAC-mediated pathways may act to maintain integrity
12
13 352 of the small intestine. TNF is involved in the pathogenesis of IBDs in humans because TNF-
14
15 353 targeted therapy is a highly effective treatment [60], and TNF is also a potent driver of epithelial
16
17 354 barrier disruption [11, 14, 17, 20, 61]. Our results clearly highlight a crucial role for LUBAC-
18
19 355 mediated linear ubiquitination in maintaining TNF-induced epithelial integrity under
20
21 356 inflammatory conditions (supplementary material, Figure S11).

22
23
24
25
26
27 357 In contrast to the LPS-induced IEC shedding model, HOIP^{IEC-Δlin} mice did not exhibit obvious
28
29 358 sensitivity to DSS-induced colitis (Figure 4A–D). In this model, mice receive oral DSS for
30
31 359 several days; however, in the LPS-induced IEC shedding model, IEC shedding is usually
32
33 360 evaluated within 1 day of LPS administration [15, 39, 40, 49]. We found that HOIP^{IEC-Δlin} mice
34
35 361 displayed mucosal inflammation within 24 h of LPS administration (Figure 1). Moreover, it is
36
37 362 suspected that administration of DSS, a direct chemical toxin to IECs, for several days leads to
38
39 363 massive disruption of IECs [53], which might suggest that augmented sensitivity to intestinal
40
41 364 inflammation and IEC death in HOIP^{IEC-Δlin} mice cannot be properly evaluated by DSS
42
43 365 administration. Therefore, the DSS-induced colitis model alone may not be suitable for probing
44
45 366 the mechanism underlying disruption of epithelial integrity within a short time. An LPS-
46
47 367 induced IEC shedding model together with DSS-induced colitis model might be more beneficial
48
49 368 for evaluating the pathogenesis of IBDs.

50
51
52
53
54 369 Pro-inflammatory macrophages accumulate and respond in a highly pro-inflammatory manner
55
56 370 to stimulation of TLR ligands after epithelial disruption induced by DSS [22, 23]. In contrast
57
58 371 to HOIP^{IEC-Δlin} mice (Figure 4), HOIP^{MYE-Δlin} mice displayed attenuated mucosal damage and

1
2
3 372 less infiltration by immune cells, as well as induction of inflammatory cytokines, upon DSS-
4
5 373 induced epithelial injury (Figure 5). We observed that loss of the LUBAC ligase activity in
6
7 374 BMDMs stimulated with LPS led to decreased production of macrophage chemoattractant
8
9
10 375 MCP-1/CCL2, as well as pro-inflammatory IL-6 and TNF, downstream of attenuated NF- κ B
11
12 376 and ERK activation (Figure 6). Since loss of the LUBAC ligase activity did not overtly augment
13
14 377 macrophage death (supplementary material, Figure S9), downregulated expression of MCP-
15
16 378 1/CCL2 (Figure 5F and 6E, F), not induction of cell death, is likely responsible for decreased
17
18
19 379 accumulation of macrophages (Figure 5D, E), which might further attenuate inflammatory
20
21
22 380 responses in DSS-treated HOIP^{MYE- Δ lin} mice. Collectively, the data suggest that linear
23
24 381 ubiquitination in macrophages augments intestinal inflammation in the event of an epithelial
25
26 382 barrier breach by promoting recruitment of macrophages to sites of damage, as well as by up-
27
28
29 383 regulating production of pro-inflammatory cytokines via activation of the NF- κ B and ERK
30
31 384 pathways (supplementary material, Figure S11).

32
33 385 **By contrast, IEC shedding** upon intraperitoneal injection of LPS was comparable in HOIP^{MYE-}
34
35 386 ^{Δ lin} and control mice (supplementary material, Figure S8A). This might be because there is no
36
37
38 387 overt difference in expression of inflammatory cytokines between LPS-treated HOIP^{MYE- Δ lin}
39
40 388 and control mice (supplementary material, Figure S8B, C). We suspected that dendritic cells,
41
42 389 effector T cells, adipocytes, and fibroblasts (in addition to macrophages) might produce IL-6
43
44 390 and TNF upon LPS injection because these cells produce these cytokines as a direct or indirect
45
46 391 response to LPS [26, 27]. Macrophages play pleiotropic roles during acute inflammation,
47
48 392 including activation of other immune cells, elimination of infectious agents, and promotion of
49
50 393 tissue regeneration, whereas prolonged inflammation delays tissue repair [22-24, 26-28]. Thus,
51
52 394 loss of LUBAC ligase activity in macrophages may prevent prolonged inflammation and
53
54 395 facilitate epithelial repair in DSS-induced colitis (Figure 5) without affecting acute
55
56 396 inflammatory responses that are necessary for tissue regeneration.
57
58
59
60

1
2
3 397 In conclusion, we show here that linear ubiquitination in IECs and macrophages plays a role
4
5 398 in the pathogenesis of IBDs. While direct epithelial injury by DSS administration is useful for
6
7 399 investigate macrophage function as the first line of defense in the innate immune system, rapid
8
9 400 and indirect IEC shedding induced by LPS administration might also be a suitable option for
10
11 401 investigating the mechanisms that maintain epithelial integrity. Linear ubiquitination in IECs
12
13 402 and macrophages functions differentially during intestinal inflammation by regulating TNF-
14
15 403 mediated epithelial integrity and macrophage pro-inflammatory responses, respectively;
16
17 404 therefore, cell-specific targeting of linear ubiquitination might be a novel approach to treating
18
19 405 IBDs.
20
21
22
23
24
25
26
27
28
29
30
31
32
33
34
35
36
37
38
39
40
41
42
43
44
45
46
47
48
49
50
51
52
53
54
55
56
57
58
59
60

For Peer Review

1
2
3 406 **Acknowledgments**
4

5 407 We thank the Center for Anatomical, Pathological and Forensic Medical Research, Kyoto
6
7 408 University Graduate School of Medicine, for preparing tissue sections. We also thank Drs. S.
8
9 409 Kuno, Y. Shinkawa, Y. Fuseya, T. Jo, Y. Takeda, I. Yanatori, H. Fujita, and M. Kim for
10
11 410 insightful discussion and advice, and Ms Y. Akasaki, Y. Hayamizu, and N. Ueno for technical
12
13 411 assistance. This work was supported by JSPS KAKENHI Grant Numbers 17H06174 and
14
15 412 18H05499 (to K. I.).
16
17
18
19 413

20
21 414 **Author contributions**
22

23 415 Y. S., Y. N., K. S., and K. I. conceived and designed the study. Y. S. performed the experiments.
24
25 416 M. O. and K. H. supported organoid culture. Y. I., K. K., K. O., and H. S. provided crucial
26
27 417 advice. Y. S. and K. I. wrote the manuscript, with contributions from all other authors.
28
29
30 418

419 **References**

- 420 1. Collaborators GBDIBD. The global, regional, and national burden of inflammatory
421 bowel disease in 195 countries and territories, 1990-2017: a systematic analysis for the Global
422 Burden of Disease Study 2017. *Lancet Gastroenterol Hepatol* 2020; **5**: 17-30.
- 423 2. Sartor RB. Mechanisms of disease: pathogenesis of Crohn's disease and ulcerative
424 colitis. *Nat Clin Pract Gastroenterol Hepatol* 2006; **3**: 390-407.
- 425 3. de Souza HS, Fiocchi C. Immunopathogenesis of IBD: current state of the art. *Nat*
426 *Rev Gastroenterol Hepatol* 2016; **13**: 13-27.
- 427 4. Chang JT. Pathophysiology of Inflammatory Bowel Diseases. *N Engl J Med* 2020;
428 **383**: 2652-2664.
- 429 5. Geremia A, Biancheri P, Allan P, *et al.* Innate and adaptive immunity in
430 inflammatory bowel disease. *Autoimmun Rev* 2014; **13**: 3-10.
- 431 6. Schey R, Danzer C, Mattner J. Perturbations of mucosal homeostasis through
432 interactions of intestinal microbes with myeloid cells. *Immunobiology* 2015; **220**: 227-235.
- 433 7. Baillie JK, Arner E, Daub C, *et al.* Analysis of the human monocyte-derived
434 macrophage transcriptome and response to lipopolysaccharide provides new insights into
435 genetic aetiology of inflammatory bowel disease. *PLoS Genet* 2017; **13**: e1006641.
- 436 8. Artis D. Epithelial-cell recognition of commensal bacteria and maintenance of
437 immune homeostasis in the gut. *Nat Rev Immunol* 2008; **8**: 411-420.
- 438 9. Turner JR. Intestinal mucosal barrier function in health and disease. *Nat Rev*
439 *Immunol* 2009; **9**: 799-809.
- 440 10. Peterson LW, Artis D. Intestinal epithelial cells: regulators of barrier function and
441 immune homeostasis. *Nat Rev Immunol* 2014; **14**: 141-153.
- 442 11. Nenci A, Becker C, Wullaert A, *et al.* Epithelial NEMO links innate immunity to
443 chronic intestinal inflammation. *Nature* 2007; **446**: 557-561.

- 1
2
3 444 12. Welz PS, Wullaert A, Vlantis K, *et al.* FADD prevents RIP3-mediated epithelial
4
5 445 cell necrosis and chronic intestinal inflammation. *Nature* 2011; **477**: 330-334.
6
7 446 13. Dannappel M, Vlantis K, Kumari S, *et al.* RIPK1 maintains epithelial homeostasis
8
9 447 by inhibiting apoptosis and necroptosis. *Nature* 2014; **513**: 90-94.
10
11 448 14. Takahashi N, Vereecke L, Bertrand MJ, *et al.* RIPK1 ensures intestinal homeostasis
12
13 449 by protecting the epithelium against apoptosis. *Nature* 2014; **513**: 95-99.
14
15 450 15. Gunther C, Buchen B, He GW, *et al.* Caspase-8 controls the gut response to
16
17 451 microbial challenges by Tnf- α -dependent and independent pathways. *Gut* 2015; **64**: 601-610.
18
19 452 16. Eftychi C, Schwarzer R, Vlantis K, *et al.* Temporally Distinct Functions of the
20
21 453 Cytokines IL-12 and IL-23 Drive Chronic Colon Inflammation in Response to Intestinal
22
23 454 Barrier Impairment. *Immunity* 2019; **51**: 367-380 e364.
24
25 455 17. Schwarzer R, Jiao H, Wachsmuth L, *et al.* FADD and Caspase-8 Regulate Gut
26
27 456 Homeostasis and Inflammation by Controlling MLKL- and GSDMD-Mediated Death of
28
29 457 Intestinal Epithelial Cells. *Immunity* 2020; **52**: 978-993 e976.
30
31 458 18. Nakanishi Y, Reina-Campos M, Nakanishi N, *et al.* Control of Paneth Cell Fate,
32
33 459 Intestinal Inflammation, and Tumorigenesis by PKC $\lambda/1$. *Cell Rep* 2016; **16**: 3297-3310.
34
35 460 19. Iwamoto M, Koji T, Makiyama K, *et al.* Apoptosis of crypt epithelial cells in
36
37 461 ulcerative colitis. *J Pathol* 1996; **180**: 152-159.
38
39 462 20. Gunther C, Martini E, Wittkopf N, *et al.* Caspase-8 regulates TNF- α -induced
40
41 463 epithelial necroptosis and terminal ileitis. *Nature* 2011; **477**: 335-339.
42
43 464 21. Smith PD, Smythies LE, Shen R, *et al.* Intestinal macrophages and response to
44
45 465 microbial encroachment. *Mucosal Immunol* 2011; **4**: 31-42.
46
47 466 22. Bain CC, Mowat AM. Macrophages in intestinal homeostasis and inflammation.
48
49 467 *Immunol Rev* 2014; **260**: 102-117.
50
51 468 23. Bain CC, Schridde A. Origin, Differentiation, and Function of Intestinal
52
53
54
55
56
57
58
59
60

- 1
2
3 469 Macrophages. *Front Immunol* 2018; **9**: 2733.
4
5 470 24. Na YR, Stakenborg M, Seok SH, *et al.* Macrophages in intestinal inflammation and
6
7 471 resolution: a potential therapeutic target in IBD. *Nat Rev Gastroenterol Hepatol* 2019; **16**:
8
9 472 531-543.
10
11
12 473 25. Akira S, Uematsu S, Takeuchi O. Pathogen recognition and innate immunity. *Cell*
13
14 474 2006; **124**: 783-801.
15
16
17 475 26. Friedrich M, Pohin M, Powrie F. Cytokine Networks in the Pathophysiology of
18
19 476 Inflammatory Bowel Disease. *Immunity* 2019; **50**: 992-1006.
20
21 477 27. Neurath MF. Cytokines in inflammatory bowel disease. *Nat Rev Immunol* 2014; **14**:
22
23 478 329-342.
24
25
26 479 28. Karin M, Clevers H. Reparative inflammation takes charge of tissue regeneration.
27
28 480 *Nature* 2016; **529**: 307-315.
29
30
31 481 29. Kirisako T, Kamei K, Murata S, *et al.* A ubiquitin ligase complex assembles linear
32
33 482 polyubiquitin chains. *EMBO J* 2006; **25**: 4877-4887.
34
35
36 483 30. Tokunaga F, Sakata S, Saeki Y, *et al.* Involvement of linear polyubiquitylation of
37
38 484 NEMO in NF- κ B activation. *Nat Cell Biol* 2009; **11**: 123-132.
39
40
41 485 31. Iwai K, Tokunaga F. Linear polyubiquitination: a new regulator of NF- κ B
42
43 486 activation. *EMBO Rep* 2009; **10**: 706-713.
44
45
46 487 32. Ikeda F, Deribe YL, Skanland SS, *et al.* SHARPIN forms a linear ubiquitin ligase
47
48 488 complex regulating NF- κ B activity and apoptosis. *Nature* 2011; **471**: 637-641.
49
50
51 489 33. Greten FR, Eckmann L, Greten TF, *et al.* IKK β links inflammation and
52
53 490 tumorigenesis in a mouse model of colitis-associated cancer. *Cell* 2004; **118**: 285-296.
54
55
56 491 34. Atreya I, Atreya R, Neurath MF. NF- κ B in inflammatory bowel disease. *J Intern*
57
58 492 *Med* 2008; **263**: 591-596.
59
60 493 35. Pasparakis M. Regulation of tissue homeostasis by NF- κ B signalling: implications

- 1
2
3 494 for inflammatory diseases. *Nat Rev Immunol* 2009; **9**: 778-788.
- 4
5 495 36. Liu T, Zhang L, Joo D, *et al.* NF- κ B signaling in inflammation. *Signal Transduct*
6
7
8 496 *Target Ther* 2017; **2**.
- 9
10 497 37. Jostins L, Ripke S, Weersma RK, *et al.* Host-microbe interactions have shaped the
11
12 498 genetic architecture of inflammatory bowel disease. *Nature* 2012; **491**: 119-124.
- 13
14
15 499 38. Vereecke L, Vieira-Silva S, Billiet T, *et al.* A20 controls intestinal homeostasis
16
17 500 through cell-specific activities. *Nat Commun* 2014; **5**: 5103.
- 18
19 501 39. Williams JM, Duckworth CA, Watson AJ, *et al.* A mouse model of pathological
20
21 502 small intestinal epithelial cell apoptosis and shedding induced by systemic administration of
22
23 503 lipopolysaccharide. *Dis Model Mech* 2013; **6**: 1388-1399.
- 24
25
26 504 40. Chassaing B, Aitken JD, Malleshappa M, *et al.* Dextran sulfate sodium (DSS)-
27
28 505 induced colitis in mice. *Curr Protoc Immunol* 2014; **104**: 15 25 11-15 25 14.
- 29
30 506 41. Sasaki Y, Iwai K. Crucial Role of Linear Ubiquitin Chain Assembly Complex-
31
32 507 Mediated Inhibition of Programmed Cell Death in TLR4-Mediated B Cell Responses and B1b
33
34 508 Cell Development. *J Immunol* 2018; **200**: 3438-3449.
- 35
36
37 509 42. Sasaki Y, Sano S, Nakahara M, *et al.* Defective immune responses in mice lacking
38
39 510 LUBAC-mediated linear ubiquitination in B cells. *EMBO J* 2013; **32**: 2463-2476.
- 40
41
42 511 43. el Marjou F, Janssen KP, Chang BH, *et al.* Tissue-specific and inducible Cre-
43
44 512 mediated recombination in the gut epithelium. *Genesis* 2004; **39**: 186-193.
- 45
46
47 513 44. Clausen BE, Burkhardt C, Reith W, *et al.* Conditional gene targeting in
48
49 514 macrophages and granulocytes using LysMcre mice. *Transgenic Res* 1999; **8**: 265-277.
- 50
51 515 45. Nakatsuji M, Minami M, Seno H, *et al.* EP4 Receptor-Associated Protein in
52
53 516 Macrophages Ameliorates Colitis and Colitis-Associated Tumorigenesis. *PLoS Genet* 2015;
54
55 517 **11**: e1005542.
- 56
57
58 518 46. Sato T, Vries RG, Snippert HJ, *et al.* Single Lgr5 stem cells build crypt-villus
59
60

- 1
2
3 519 structures in vitro without a mesenchymal niche. *Nature* 2009; **459**: 262-265.
4
5 520 47. Peltzer N, Rieser E, Taraborrelli L, *et al.* HOIP deficiency causes embryonic
6
7 521 lethality by aberrant TNFR1-mediated endothelial cell death. *Cell Rep* 2014; **9**: 153-165.
8
9
10 522 48. Peltzer N, Darding M, Montinaro A, *et al.* LUBAC is essential for embryogenesis
11
12 523 by preventing cell death and enabling haematopoiesis. *Nature* 2018; **557**: 112-117.
13
14 524 49. Jones LG, Vaida A, Thompson LM, *et al.* NF- κ B2 signalling in enteroids
15
16 525 modulates enterocyte responses to secreted factors from bone marrow-derived dendritic cells.
17
18 526 *Cell Death Dis* 2019; **10**: 896.
19
20 527 50. Taraborrelli L, Peltzer N, Montinaro A, *et al.* LUBAC prevents lethal dermatitis by
21
22 528 inhibiting cell death induced by TNF, TRAIL and CD95L. *Nat Commun* 2018; **9**: 3910.
23
24 529 51. Tang Y, Joo D, Liu G, *et al.* Linear ubiquitination of cFLIP induced by LUBAC
25
26 530 contributes to TNF α -induced apoptosis. *J Biol Chem* 2018; **293**: 20062-20072.
27
28 531 52. Watson AJ, Hughes KR. TNF- α -induced intestinal epithelial cell shedding:
29
30 532 implications for intestinal barrier function. *Ann N Y Acad Sci* 2012; **1258**: 1-8.
31
32 533 53. Eichele DD, Kharbanda KK. Dextran sodium sulfate colitis murine model: An
33
34 534 indispensable tool for advancing our understanding of inflammatory bowel diseases
35
36 535 pathogenesis. *World J Gastroenterol* 2017; **23**: 6016-6029.
37
38 536 54. Gantke T, Sriskantharajah S, Sadowski M, *et al.* I κ B kinase regulation of the TPL-
39
40 537 2/ERK MAPK pathway. *Immunol Rev* 2012; **246**: 168-182.
41
42 538 55. Webb LV, Ventura S, Ley SC. ABIN-2, of the TPL-2 Signaling Complex,
43
44 539 Modulates Mammalian Inflammation. *Trends Immunol* 2019; **40**: 799-808.
45
46 540 56. Oikawa D, Sato Y, Ohtake F, *et al.* Molecular bases for HOIPINs-mediated
47
48 541 inhibition of LUBAC and innate immune responses. *Commun Biol* 2020; **3**: 163.
49
50 542 57. Vereecke L, Beyaert R, van Loo G. Enterocyte death and intestinal barrier
51
52 543 maintenance in homeostasis and disease. *Trends Mol Med* 2011; **17**: 584-593.
53
54
55
56
57
58
59
60

- 1
2
3 544 58. Kumari S, Redouane Y, Lopez-Mosqueda J, *et al.* Sharpin prevents skin
4
5 545 inflammation by inhibiting TNFR1-induced keratinocyte apoptosis. *Elife* 2014; **3**.
6
7 546 59. Rickard JA, Anderton H, Etemadi N, *et al.* TNFR1-dependent cell death drives
8
9 547 inflammation in Sharpin-deficient mice. *Elife* 2014; **3**.
10
11
12 548 60. Neurath MF. Current and emerging therapeutic targets for IBD. *Nat Rev*
13
14 549 *Gastroenterol Hepatol* 2017; **14**: 269-278.
15
16
17 550 61. Pott J, Kabat AM, Maloy KJ. Intestinal Epithelial Cell Autophagy Is Required to
18
19 551 Protect against TNF-Induced Apoptosis during Chronic Colitis in Mice. *Cell Host Microbe*
20
21 552 2018; **23**: 191-202 e194.
22
23
24 553
25
26 554
27
28
29
30
31
32
33
34
35
36
37
38
39
40
41
42
43
44
45
46
47
48
49
50
51
52
53
54
55
56
57
58
59
60

1
2
3 **555 Figure legends**
4

5 **556 Figure 1. Deletion of epithelial linear ubiquitination activity sensitizes mice to mucosal**
6
7 **557 inflammation and IEC death upon intraperitoneal administration of LPS.**

8
9
10 **558 (A)** Representative pictures (left) and quantification of colon length (right) in control and
11
12 **559** HOIP^{IEC-Δlin} mice at the indicated times post-LPS treatment (n=3–5). ns, not significant.

13
14
15 **560 (B)** H&E staining of distal colon sections from control and HOIP^{IEC-Δlin} mice 24 h post-LPS
16
17 **561** administration (n=3). Scale bars, 50 μm.

18
19
20 **562 (C)** Immunohistochemical staining for CD45 and F4/80 in the distal colon 4 h post-LPS
21
22 **563** injection (n=3). Data from untreated control (UT) and HOIP^{IEC-Δlin} mice are also shown (n=3).

23
24 **564** Yellow arrow heads depict cells positive for each marker. Scale bars, 50 μm.

25
26
27 **565 (D)** Quantification of immune cells in (C) (n=12 fields per group). Data from untreated control
28
29 **566** and HOIP^{IEC-Δlin} mice are also shown (n=12 fields per group).

30
31
32 **567 (E)** Immunohistochemical staining for cleaved caspase 3 (Cl. Caspase3) in distal colon sections
33
34 **568** 4 h post-LPS treatment (n=3). Data from untreated control and HOIP^{IEC-Δlin} mice are also shown
35
36 **569** (n=3). Scale bars, 50 μm.

37
38
39 **570 (F)** Immunofluorescence staining for TUNEL (green), E-cadherin (red), and DAPI (blue) in
40
41 **571** distal colon sections 4 h post-LPS treatment (n=3). Data from untreated control and HOIP^{IEC-}
42
43 **572** ^{Δlin} mice are also shown (n=3). Scale bars, 50 μm.

44
45
46 **573** Statistical significance was determined by two-way ANOVA with Bonferroni's post-hoc test
47
48 **574** (A, D). *P < 0.05, **P < 0.01, ***P < 0.005, ****P < 0.001.

49
50 **575**

51
52
53 **576 Figure 2. Intestinal epithelial organoids lacking LUBAC catalytic activity show evidence**
54
55 **577 of apoptosis upon treatment with TNF.**

56
57 **578 (A)** Representative images (top) obtained under a bright field microscope, SYTOX Green
58
59 **579** staining, and Hoechst 33342 staining of organoids from control and HOIP^{IEC-Δlin} IECs treated

1
2
3 580 with PBS, LPS (100 ng/ml), or TNF (25 ng/ml) for 24 h. Percentage (bottom) of SYTOX Green-
4
5 581 positive organoids among total organoids. Data were obtained from a total of 30–50 organoids
6
7 582 per group. Experiments were performed at least three times independently. Scale bars, 100 μ m.
8
9
10 583 (B) ELISA to detect serum TNF levels in control and HOIP^{IEC- Δ lin} mice after intraperitoneal
11
12 584 injection of LPS (n=3).
13
14 585 (C) qRT-PCR analysis of *Tnf* mRNA levels in colon tissue from control and HOIP^{IEC- Δ lin} mice
15
16 586 after LPS administration (n=6). Data are normalized to expression of *Gapdh* mRNA.
17
18 587 (D) Organoids derived from control and HOIP^{IEC- Δ lin} mice were stimulated with TNF (40 ng/ml),
19
20 588 or pre-treated with ZVAD (20 μ M) for 1 h followed by treatment with TNF (40 ng/ml) for the
21
22 589 indicated times. Cell lysates were immunoblotted with the indicated antibodies. Tubulin was
23
24 590 used as a loading control.
25
26
27 591 (E) Organoids from control and HOIP^{IEC- Δ lin} mice were stimulated with TNF (40 ng/ml) for the
28
29 592 indicated times. Cell lysates were immunoblotted with the indicated antibodies. Tubulin was
30
31 593 used as a loading control.
32
33
34 594 (F) Organoids from control and HOIP^{IEC- Δ lin} IECs were stimulated with TNF (25 ng/ml) for the
35
36 595 indicated times, followed by qRT-PCR analysis of NF- κ B target gene mRNA (n=3). Data are
37
38 596 normalized to expression of *Gapdh* mRNA.
39
40
41 597 A representative image of an immunoblot from at least three independent experiments is shown.
42
43 598 Statistical significance was determined by two-way ANOVA with Bonferroni's post-hoc test
44
45 599 (A, B, C, F). *P < 0.05, ***P < 0.005, ****P < 0.001.
46
47
48
49
50
51

52
53 601 **Figure 3. TNF plays a role in mucosal inflammation and IEC death in LPS-treated mice**
54
55 602 **lacking linear ubiquitination activity in IECs.**

56
57 603 (A) Representative pictures (left) and quantification of colon length (right) in control and
58
59 604 HOIP^{IEC- Δ lin} mice at the indicated times after intraperitoneal administration of TNF (n=3).

1
2
3 605 (B) H&E staining of distal colon sections from control and HOIP^{IEC-Δlin} mice 24 h after TNF
4
5
6 606 treatment (n=3). Scale bars, 50 μm.

7
8 607 (C) Immunohistochemical staining for CD45 and F4/80 in distal colon sections 4 h after
9
10 608 injection of TNF (n=3). Yellow arrow heads indicate cells positive for each marker. Scale bars,
11
12 609 50 μm.

13
14
15 610 (D) Quantification of immune cells in (C) (n=12 fields per group).

16
17 611 (E) Immunohistochemical staining for cleaved caspase 3 in distal colon from control and
18
19 612 HOIP^{IEC-Δlin} mice 4 h after TNF treatment (n=3). Scale bars, 50 μm.

20
21
22 613 (F) HOIP^{IEC-Δlin} mice were injected intraperitoneally with isotype control IgG or an anti-TNF
23
24 614 antibody 1 h prior to intraperitoneal injection of LPS. Representative pictures (left) and
25
26 615 quantification of colon length (right) in isotype control- or anti-TNF-treated HOIP^{IEC-Δlin} mice
27
28 616 at the indicated times after LPS injection (n=3).

29
30
31 617 (G) H&E staining of the distal colon sections from isotype control- or anti-TNF-treated
32
33 618 HOIP^{IEC-Δlin} mice 24 h post-LPS administration (n=3). Scale bars, 50 μm.

34
35
36 619 (H) Immunohistochemical staining for CD45 and F4/80 in distal colon sections from isotype
37
38 620 control- or anti-TNF-treated HOIP^{IEC-Δlin} mice 4 h post-LPS (n=3). Yellow arrow heads depict
39
40 621 cells positive for each marker. Scale bars, 50 μm.

41
42
43 622 (I) Quantification of immune cells in (H) (n=12 fields per group).

44
45
46 623 (J) Immunohistochemical staining for cleaved caspase 3 in distal colon sections from isotype
47
48 624 control- or anti-TNF-treated HOIP^{IEC-Δlin} mice 4 h after LPS administration (n=3). Scale bars,
49
50 625 50 μm.

51
52
53 626 Statistical significance was determined by two-way ANOVA with Bonferroni's post-hoc test
54
55 627 (A, F), or by a two-tailed unpaired Student's t test (D, I). *P < 0.05, **P < 0.01, ****P < 0.001.

56
57 628

58
59
60 629 **Figure 4. Defects in epithelial linear ubiquitination activity do not overtly affect the**

1
2
3 630 **severity of DSS-induced colitis.**

4
5 631 (A) Control and HOIP^{IEC-Δlin} mice were fed 2.0% DSS for 7 days. They were then fed regular
6
7
8 632 water for 2 days. Body weight changes in control (n=7) and HOIP^{IEC-Δlin} mice (n=7) during DSS
9
10 633 treatment. BW, body weight; IBW, initial body weight.

11
12 634 (B) Representative pictures (left) and quantification of colon length (right) in DSS-treated
13
14
15 635 control (n=7) and HOIP^{IEC-Δlin} mice (n=7). Data from untreated control and HOIP^{IEC-Δlin} mice
16
17 636 are also shown (n=6).

18
19
20 637 (C) H&E staining (left) and histological damage scores (right) for distal colon sections from
21
22 638 control and HOIP^{IEC-Δlin} mice treated with DSS (n=7). Scale bars, 50 μm.

23
24 639 (D) qRT-PCR analysis of inflammatory cytokine and chemokine expression in colon tissue
25
26
27 640 from control (n=8) and HOIP^{IEC-Δlin} mice (n=6) subjected to DSS-induced colitis. Data from
28
29 641 untreated control and HOIP^{IEC-Δlin} mice are also shown (n=3). Data are normalized to expression
30
31 642 of *Gapdh* mRNA.

32
33
34 643 (E) Immunohistochemical staining for cleaved caspase 3 and immunofluorescence staining for
35
36 644 TUNEL in distal colon sections from control and HOIP^{IEC-Δlin} mice treated with DSS (n=3).
37
38 645 Yellow arrow heads depict cells positive for cleaved caspase 3. Scale bars, 50 μm.

39
40
41 646 Statistical significance was determined by two-way ANOVA with Bonferroni's post-hoc test
42
43 647 (A, B, D), or by a two-tailed unpaired Student's t test (C).

44
45 648

46
47
48 649 **Figure 5. Loss of linear ubiquitination activity in macrophages results in mild colitis after**
49
50 650 **DSS treatment.**

51
52 651 (A) Body weight changes in control (n=10) and HOIP^{MYE-Δlin} (n=13) mice during DSS treatment.

53
54 652 (B) Representative pictures (left) and quantification of colon length (right) in DSS-treated
55
56
57 653 control (n=8) and HOIP^{MYE-Δlin} (n=10) mice. Data from untreated control and HOIP^{MYE-Δlin} mice
58
59 654 are also shown (n=6).

1
2
3 655 (C) H&E staining (left) and histological damage scores (right) for distal colon from control and
4
5 656 HOIP^{MYE-Δlin} mice treated with DSS (n=5). Scale bars, 50 μm.

7
8 657 (D) Immunohistochemical staining for CD45, F4/80, B220, and CD3 in distal colon sections
9
10 658 from DSS-treated control and HOIP^{MYE-Δlin} mice (n=5). Yellow arrow heads indicate cells
11
12 659 positive for each marker. Scale bars, 50 μm.

14
15 660 (E) Quantification of immune cells in (D) (n=10 fields per group). Data from control and
16
17 661 HOIP^{MYE-Δlin} mice under basal conditions are also shown (n=6 fields per group).

19
20 662 (F) qRT-PCR analysis of inflammatory cytokine and chemokine expression in colon tissue from
21
22 663 DSS-treated control (n=5) and HOIP^{MYE-Δlin} (n=6) mice. Data from control and HOIP^{MYE-Δlin}
23
24 664 mice under basal conditions are also shown (n=3). Data are normalized to expression of *Gapdh*
25
26 665 mRNA.

28
29 666 Statistical significance was determined by two-way ANOVA with Bonferroni's post-hoc test
30
31 667 (A, B, E, F), or by a two-tailed unpaired Student's t test (C). *P < 0.05, **P < 0.01, ****P < 0.001.

33
34 668

35
36 669 **Figure 6. Deficiency of linear ubiquitination in macrophages impairs NF-κB- and ERK-**
37
38 670 **mediated inflammatory responses upon TLR stimulation.**

39
40
41 671 (A) BMDMs derived from control and HOIP^{MYE-Δlin} mice were stimulated with TNF (1 ng/ml)
42
43 672 for the indicated times. Cell lysates were immunoblotted with the indicated antibodies. Tubulin
44
45 673 was used as a loading control.

47
48 674 (B and C) Control and HOIP^{MYE-Δlin} BMDMs were stimulated with LPS (10 ng/ml) for the
49
50 675 indicated times. Whole cell lysates were immunoblotted with the indicated antibodies. Tubulin
51
52 676 was used as a loading control.

54
55 677 (D) BMDMs from WT mice were pre-treated with DMSO or HOIPin-8 (10 μM) for 30 min,
56
57 678 and then stimulated with LPS (10 ng/ml) for the indicated times. Whole cell lysates were
58
59 679 immunoblotted with the indicated antibodies. Tubulin was used as a loading control.

1
2
3 680 (E) ELISA to detect IL-6, TNF, and MCP-1/CCL2 produced by control and HOIP^{MYE-Δlin}
4
5 681 BMDMs stimulated with LPS (10 ng/ml) for 24 h (n=3).
6
7
8 682 (F) BMDMs from WT mice were pre-treated for 30 min with DMSO or HOIPin-8 (10 μM),
9
10 683 and then stimulated with LPS (10 ng/ml) for 24 h. Secreted IL-6, TNF, and MCP-1/CCL2 were
11
12 684 quantified by ELISA (n=3).
13
14
15 685 (G) BMDMs from WT mice were pre-treated with DMSO or a MEK inhibitor (0.5 μM) for 10
16
17 686 min, and then stimulated with LPS (10 ng/ml) for 24 h. Secreted IL-6, TNF, and MCP-1/CCL2
18
19 687 were quantified by ELISA (n=3).
20
21
22 688 (H) Control and HOIP^{MYE-Δlin} BMDMs were stimulated for 24 h with the indicated TLR ligands.
23
24 689 Secreted IL-6 was measured by ELISA (n=3). The concentrations of the TLR ligands were as
25
26 690 follows: Poly(I:C) (2 μg/ml), CpG-B (5 μM), and Pam3CSK4 (1 μg/ml).
27
28
29 691 A representative image of an immunoblot from at least three independent experiments is shown.
30
31 692 Statistical significance was determined by a two-tailed unpaired Student's t test (E, F, G, H).
32
33 693 *P < 0.05, **P < 0.01, ***P < 0.005, ****P < 0.001.
34
35
36 694

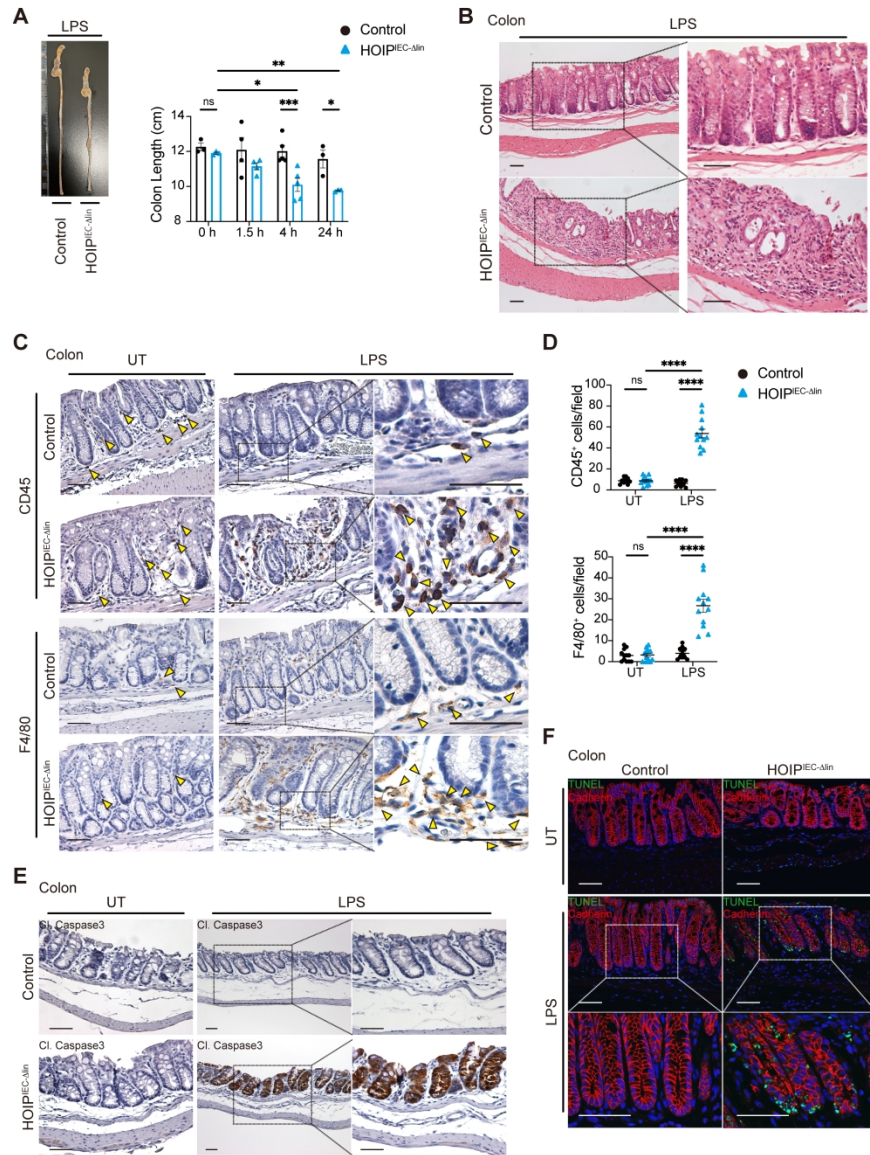


Figure 1

Figure 1

437x588mm (197 x 197 DPI)

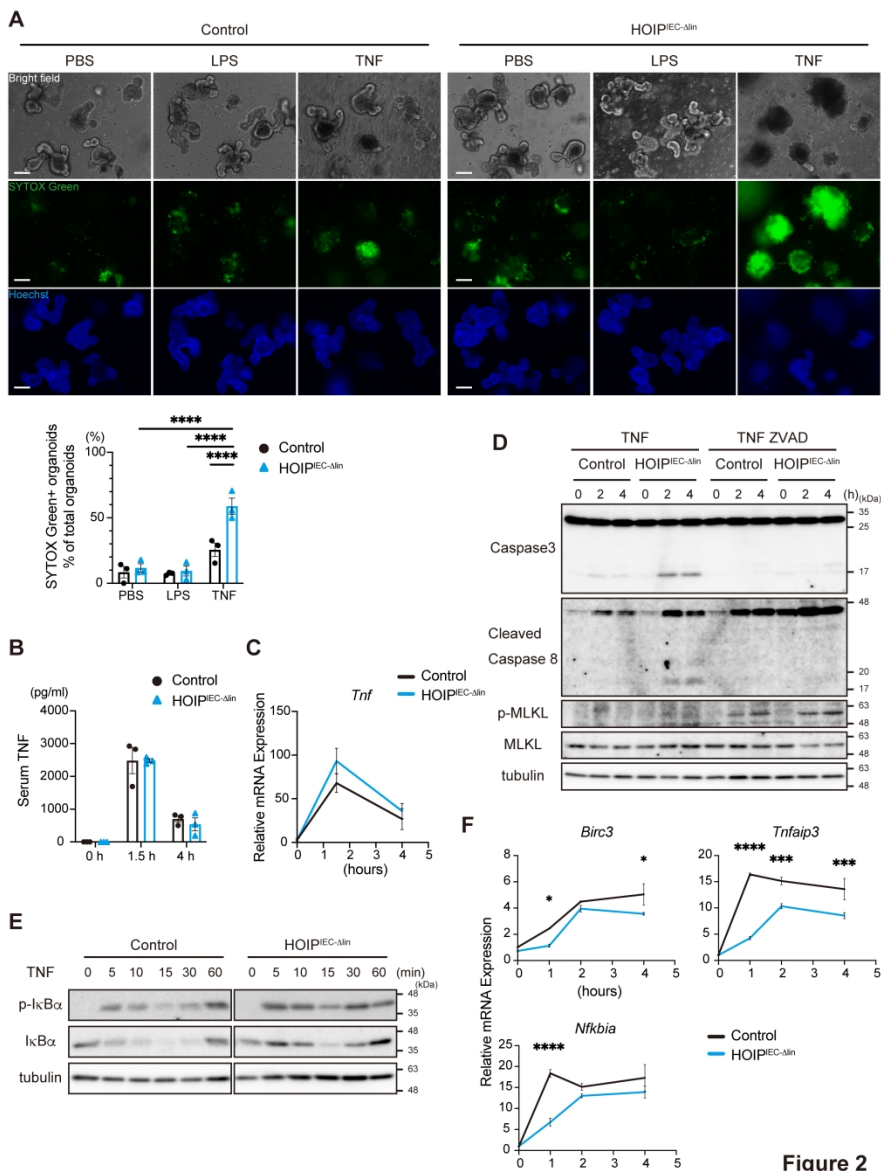


Figure 2

437x588mm (197 x 197 DPI)

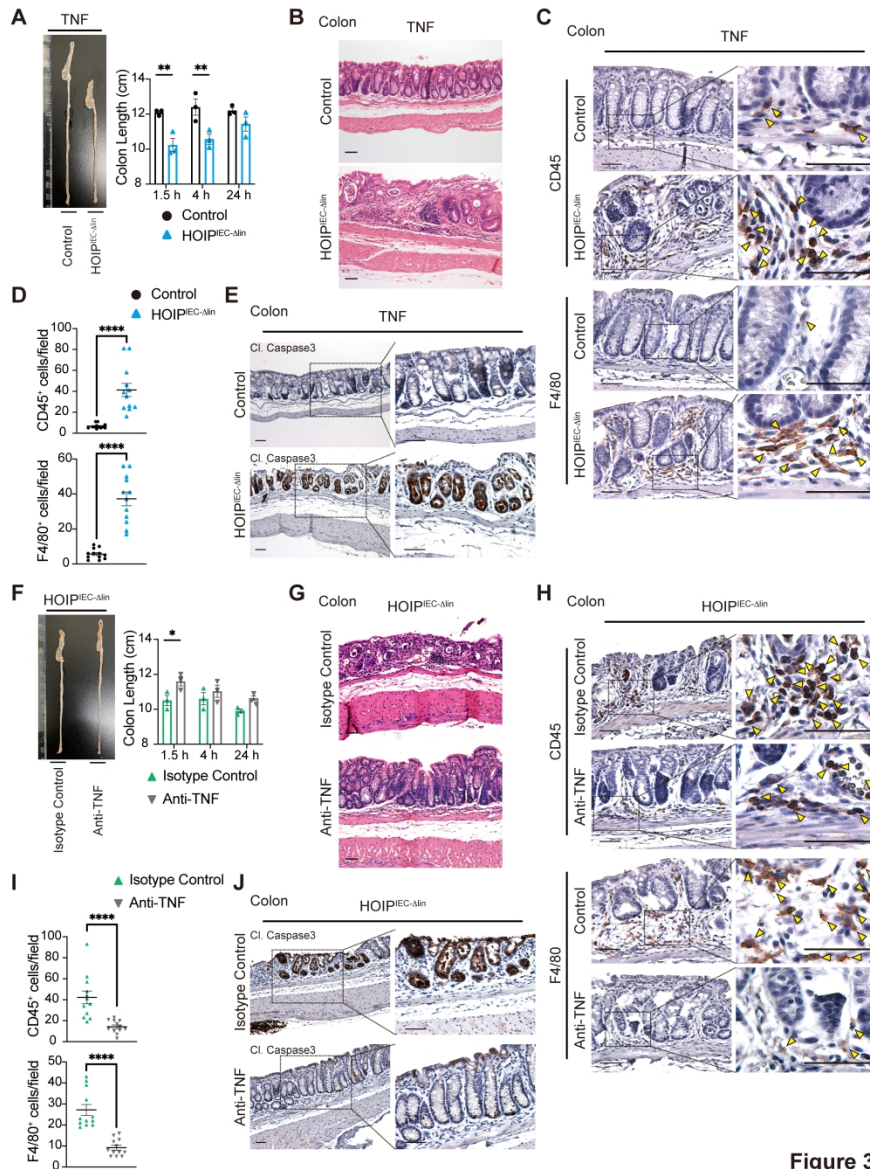


Figure 3

Figure 3

437x588mm (197 x 197 DPI)

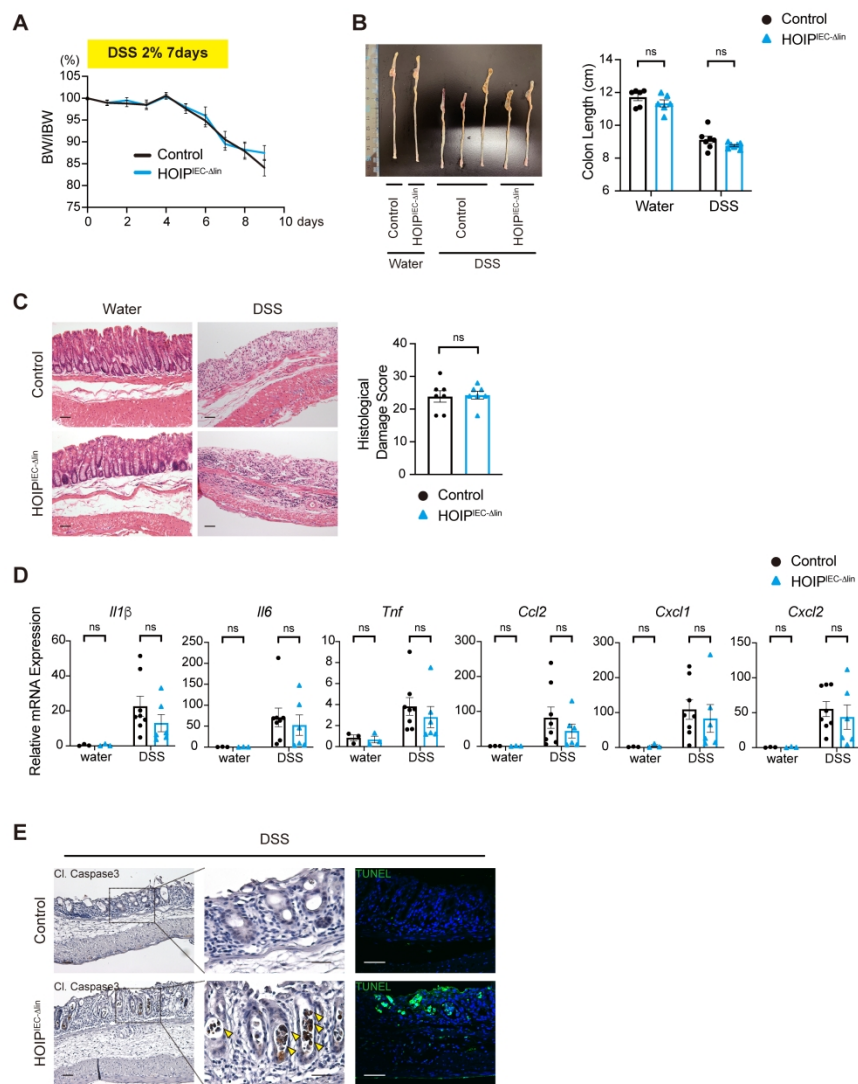


Figure 4

Figure 4

437x588mm (197 x 197 DPI)

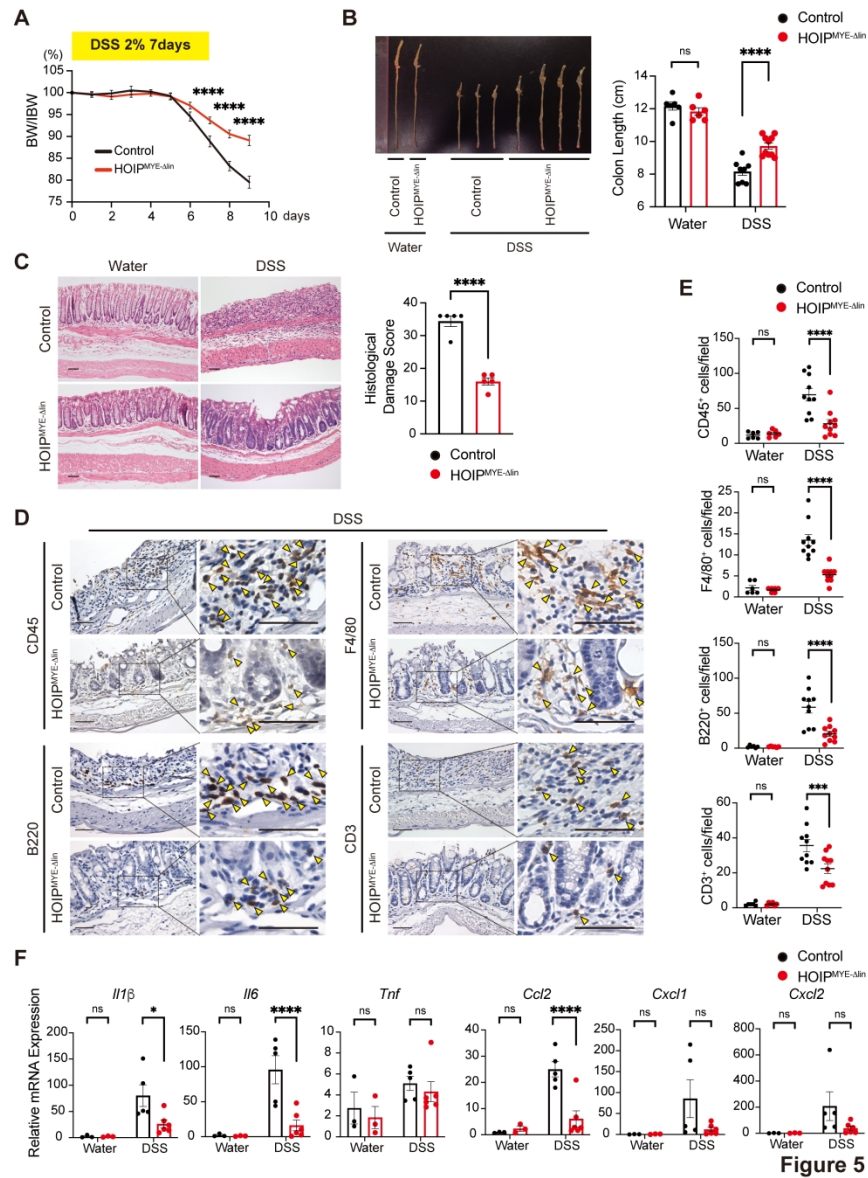


Figure 5

437x588mm (197 x 197 DPI)

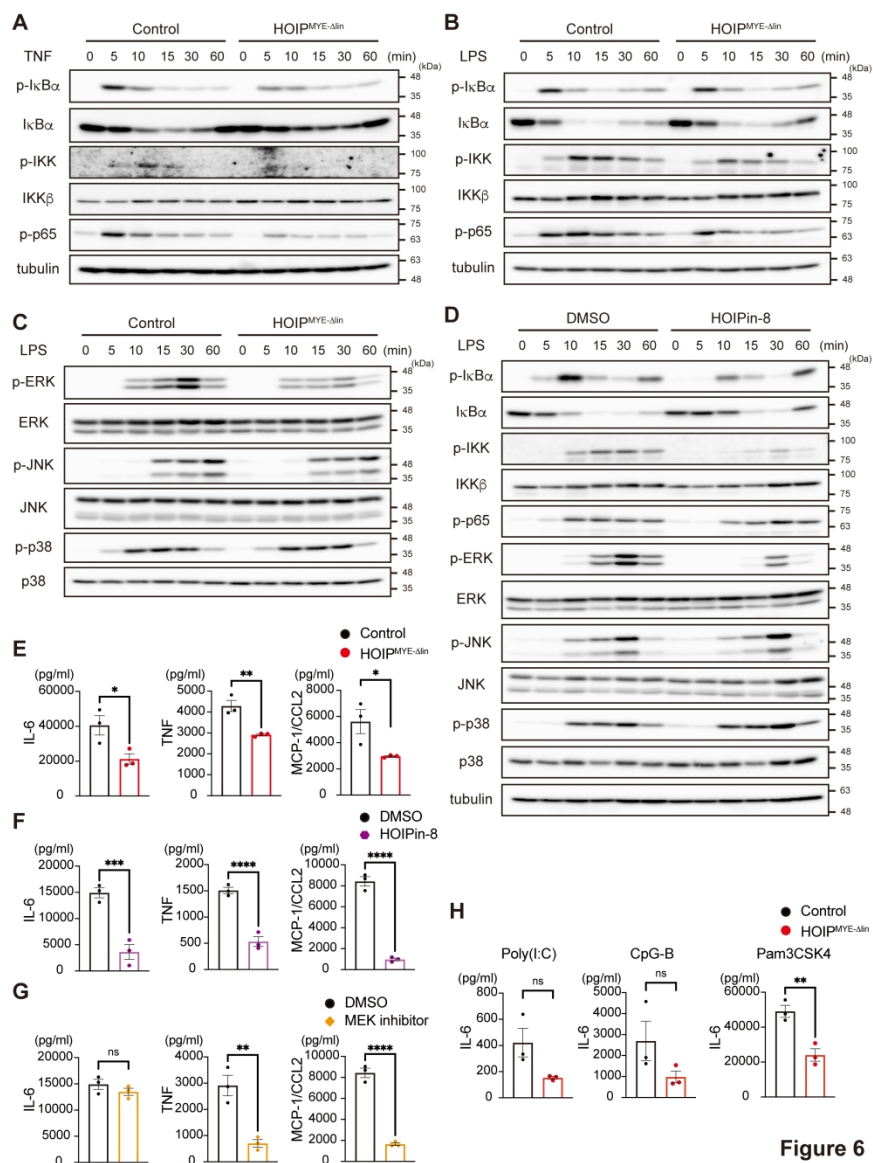


Figure 6

Figure 6

437x588mm (197 x 197 DPI)

Supporting Information

Supplementary materials and methods

Antibodies

The following antibodies were used for immunohistochemistry: anti-CD45 (clone 30F-11, cat. no. 550539, 1:100 dilution; BD Biosciences, Franklin Lakes, NJ, USA), anti-F4/80 (clone CI:A3-1, cat. no. MCA497GA, 1:100 dilution; Bio-Rad, Hercules, CA, USA), anti-cleaved caspase-3 (cat. no. 9661, 1:100 dilution; Cell Signaling Technology, Danvers, MA, USA), anti-CD45R/B220 (clone RA3-6B2, cat. no. 103202, 1:200 dilution; BioLegend, San Diego, CA, USA), and anti-CD3 ϵ (clone M-20, cat. no. SC-1127, 1:400 dilution; Santa Cruz Biotechnology, Dallas, TX, USA). The following antibodies were used for immunofluorescence staining: anti-F4/80 (cat. no. 70076, 1:100 dilution; Cell Signaling Technology), anti-E-Cadherin (cat. no. GTX100443, 1:50 dilution; Gene Tex, Irvine, CA, USA), anti-CD3 ϵ (clone M-20, cat. no. SC-1127, 1:400 dilution; Santa Cruz Biotechnology); anti-rabbit IgG AlexaFlour 488 (cat. no. A-11034), anti-rabbit IgG-AlexaFluor 546 (cat. no. A-11035), and anti-goat IgG AlexaFlour 488 (cat. no. A-11055) (all from Invitrogen, Waltham, MA, USA; 1:200 dilution). The following antibodies were used for immunoblotting: anti-I κ B α (cat. no. 4812), anti-p-I κ B α (cat. no. 9246), anti-IKK β (cat. no. 8943), anti-p-IKK (cat. no. 2697), anti-p-p65 (cat. no. 3033), anti-ERK (cat. no. 9102), anti-p-ERK (cat. no. 9101), anti-JNK (cat. no. 9258), anti-p-JNK (cat. no. 4668), anti-p38 (cat. no. 9212), anti-p-p38 (cat. no. 9211), anti-caspase-3 (cat. no. 9662), anti-cleaved caspase-8 (cat. no. 8592) (all from Cell Signaling Technology; 1:2000 dilution); anti-MLKL (phosphor S345) (cat. no. ab196436, 1:2000 dilution; abcam, Waltham, MA, USA), anti-MLKL (cat. no. SAB1302339, 1:250 dilution; Sigma-Aldrich, St. Louis, MO, USA); anti-mouse HOIP (clone N1), anti-HOIL-1L (clone 2E2), anti-SHARPIN (clone lot1) (all produced in-house; 1:2000 dilution); β -actin (clone AC-74, cat. no. A5316, 1:5000 dilution; Sigma-Aldrich), α -tubulin

1
2
3 26 (clone DM1A, cat. no. CLT9002, 1:5000 dilution; CEDARLANE, Ontario, Canada),
4
5 27 HRP-linked anti-rabbit IgG (cat. no. NA934V, 1:5000 dilution; Cytiva, Marlborough, MA,
6
7
8 28 USA), and HRP-linked anti-mouse IgG (cat. no. 7076, Cell Signaling Technology; 1:5000
9
10 29 dilution). The following antibodies were used for flow cytometry analysis:
11
12 30 APC-Cy7-anti-CD45 (clone 30F-11, cat. no. 103116, 1:100 dilution), APC-anti-F4/80 (clone
13
14 31 BM8, cat. no. 123115, 1:200 dilution), PE-Cy7-anti-CD11b (clone M1/70, cat. no. 101215,
15
16 32 1:200 dilution), PE-Cy7-anti-CD19 (clone 6D5, cat. no. 115520, 1:200 dilution),
17
18 33 PerCP-Cy5-5-anti-CD4 (clone GK1.5, cat. no. 100434, 1:200 dilution), PE-Cy7-anti-CD8a
19
20 34 (clone 53-6.7, cat. no. 100722, 1:200 dilution), APC-anti-CD69 (clone H1.2F3, cat. no.
21
22 35 104513, 1:200 dilution), APC-anti-CD62L (clone MEL-14, cat. no. 104412, 1:200 dilution),
23
24 36 PE-anti-CD44 (clone IM7, cat. no. 103008, 1:200 dilution), streptavidin-PerCP-Cy5-5 (cat.
25
26 37 no. 405213, 1:400 dilution) (all from BioLegend); PE-anti-FAS (clone Jo2, cat. no. 554258,
27
28 38 1:200 dilution; BD Biosciences), FITC-anti-TCRb (clone H57-597, cat. no. 11-5961-82,
29
30 39 1:200 dilution; eBioscience, San Diego, CA, USA), PE-anti-CD25 (clone PC61.5, cat. no.
31
32 40 12-0251-81, 1:200 dilution, eBioscience), and Biotin-anti-PNA (cat. no. B-1075, 1:400
33
34 41 dilution, Vector Laboratories, Newark, CA, USA).
35
36
37
38
39
40
41
42

43 **Histological assessment of DSS-induced colitis**

44 The histological damage score was determined based on three parameters. Inflammation
45 severity was scored as 0–3, extent of inflammation was scored as 0–3, and crypt damage was
46 scored as 0–4. The sum of each parameter was multiplied by percentage involvement (0% =
47 0; $\leq 25\%$ = 1; $\leq 50\%$ = 2; $\leq 75\%$ = 3; and $\leq 100\%$ = 4) to yield the histological damage score.
48
49

50 **Immunostaining**

51 Immunohistochemical staining was performed using an ImmPRESS Polymer Detection Kit
52
53
54
55
56
57
58
59
60

1
2
3 51 (Vector Laboratories). Paraffin-embedded sections were deparaffinized, rehydrated, and then
4
5 52 immersed in citrate buffer (pH 6.0) for 15 min in a microwave processor (MI-77; Azumayaika,
6
7 53 Tokyo, Japan) for antigen retrieval. After blocking with normal goat or horse serum blocking
8
9 54 solution (Vector Laboratories), sections were incubated with primary antibody overnight at
10
11 55 4°C. The stained sections were incubated for 30 min at room temperature with ImmPRESS
12
13 56 Polymer Reagent (Vector Laboratories), then colored with diaminobenzidine substrate
14
15 57 (DAKO, Carpinteria, CA, USA) and counterstained with hematoxylin. Endogenous
16
17 58 peroxidase was quenched for 10 min at room temperature in 0.45% H₂O₂ in methanol or 3%
18
19 59 H₂O₂ in water. Prior to immunofluorescence staining, antigen retrieval was performed as
20
21 60 described above. After sections were blocked for 1 h with blocking buffer (2% BSA and 0.1%
22
23 61 Triton X-100 in PBS) containing 5% goat serum, sections were incubated overnight at 4°C
24
25 62 with primary antibodies diluted in blocking buffer. The stained sections were incubated for 1
26
27 63 h at room temperature with fluorescent dye-conjugated anti-rabbit IgG-AlexaFluor 488 or
28
29 64 anti-goat IgG-AlexaFluor 488 in blocking buffer. For preservation, labeled sections were
30
31 65 mounted in ProLong Glass Antifade Mountant (Invitrogen). TUNEL staining was performed
32
33 66 using an In Situ Cell Death Detection Kit, Fluorescein (Sigma-Aldrich). Prior to co-staining
34
35 67 for TUNEL and for E-Cadherin, antigen retrieval was performed as described above. Then,
36
37 68 sections were incubated for 1 h at 37°C with TUNEL reaction mixture. After blocking as
38
39 69 described above, sections were incubated overnight at 4°C with an anti-E-Cadherin antibody
40
41 70 in blocking buffer. The stained sections were then incubated for 1 h at room temperature with
42
43 71 fluorescent dye-conjugated anti-rabbit IgG-AlexaFluor 546 in blocking buffer. For
44
45 72 preservation, labeled sections were mounted in ProLong Glass Antifade Mountant
46
47 73 (Invitrogen). DAPI was used to stain nuclei.
48
49
50
51
52
53
54
55
56
57
58
59
60

75 **IEC isolation and organoid culture**

1
2
3 76 The distal 10 cm segment of the small intestine or the whole colon was opened longitudinally
4
5 77 and minced. The intestinal segments were washed with cold PBS and incubated at 4°C for 40
6
7 78 min with PBS containing 5 mM EDTA and 10% FBS (whole colon was incubated for 60 min)
8
9 79 with rocking. After removal of the EDTA medium, the tissue fragments were shaken
10
11 80 vigorously in cold PBS to detach the villous and crypt fractions, and then passed through a
12
13 81 100 µm cell strainer (Corning, Glendale, AZ, USA). For IEC isolation, the flow-through were
14
15 82 pelleted and lysed for RNA extraction or immunoblotting. For organoid culture, the
16
17 83 flow-through from the small intestine was filtered through a 70 µm cell strainer (Corning) to
18
19 84 remove villous material. Isolated crypts were mixed with 50 µl of Matrigel (Corning) and
20
21 85 plated in 24-well plates. After the Matrigel polymerized, 500 µl of IntestiCult Organoid
22
23 86 Growth Medium (STEMCELL Technologies, Vancouver, Canada) was added to each well,
24
25 87 followed by cultivation at 37°C/5% CO₂.
26
27
28
29
30
31
32
33

34 **Enrichment of peritoneal macrophages**

35
36 90 Peritoneal macrophages were obtained by flushing out the peritoneal cavity with 10 ml of
37
38 91 cold PBS. The collected medium was plated into 6 or 12 well plates for 2 h. Non-adherent
39
40 92 cells were washed away with PBS and the attached cells were used as peritoneal macrophages.
41
42 93 Primary cells from each organ were washed with Gey's Buffer to deplete red blood cells.
43
44
45
46

47 **Immunoblotting**

48
49 96 Cells were lysed with lysis buffer containing 50 mM Tris-HCl (pH 7.5), 150 mM NaCl, 1%
50
51 97 Triton X-100, 2 mM PMSF, and protease inhibitor cocktail (Sigma-Aldrich). **Organoids were**
52
53 98 **lysed in RIPA buffer (50 mM Tris-HCl (pH 8.0), 150 mM NaCl, 1% Triton X-100, 0.1% SDS,**
54
55 99 **0.1% sodium deoxycholate, 2 mM PMSF, and protease inhibitor cocktail; (Sigma-Aldrich)).**
56
57
58
59 100 Lysates were centrifuged at 15,000 rpm for 10 min at 4°C, and the supernatant was used in
60

1
2
3 101 subsequent steps. To examine phosphorylation, a phosphatase inhibitor cocktail (Nacalai
4
5 102 Tesque, Kyoto, Japan) was added. To assess the protein translocating to the nucleus, total cell
6
7 103 lysates were obtained by incubation in SDS sample buffer. The cell lysates were then
8
9 104 separated by SDS-PAGE and transferred onto PVDF membranes (Merck Millipore,
10
11 105 Burlington, MA, USA). After blocking in Tris-buffered saline containing 0.1% Tween 20 and
12
13 106 5% nonfat dry milk, the membrane was immunoblotted with the indicated primary antibodies,
14
15 107 followed by the corresponding secondary antibodies. The membranes were visualized by
16
17 108 enhanced chemiluminescence and analyzed by an LAS3000 or LAS4000mini instrument (GE
18
19 109 Healthcare, Chicago, IL, USA).
20
21
22
23
24
25

26 111 **Quantitative RT-PCR analysis**

27
28 112 Total RNA from IECs or organoids was extracted using an RNeasy Mini Kit (Qiagen, Venlo,
29
30 113 Netherlands). To extract RNA from colon tissue, 5 mm segments taken from between the
31
32 114 middle and distal third of the colon were used. Pre-purified RNAs were extracted using
33
34 115 ISOGEN (NIPPON GENE, Tokyo, Japan), and then subjected to column-based purification
35
36 116 using an RNeasy Mini Kit (Qiagen). Total RNA was reverse transcribed into cDNA using a
37
38 117 High Capacity RNA-to-cDNA Kit (Thermo Fisher Scientific). Real-time PCR was performed
39
40 118 with Power SYBR Green PCR Master Mix (Thermo Fisher Scientific) and a ViiA7 Real-Time
41
42 119 PCR system (Applied Biosystems, Waltham, MA, USA). The results were analyzed by the
43
44 120 $\Delta\Delta$ CT method. The sequences of the primers used for qPCR are listed in Table S1.
45
46
47
48
49
50

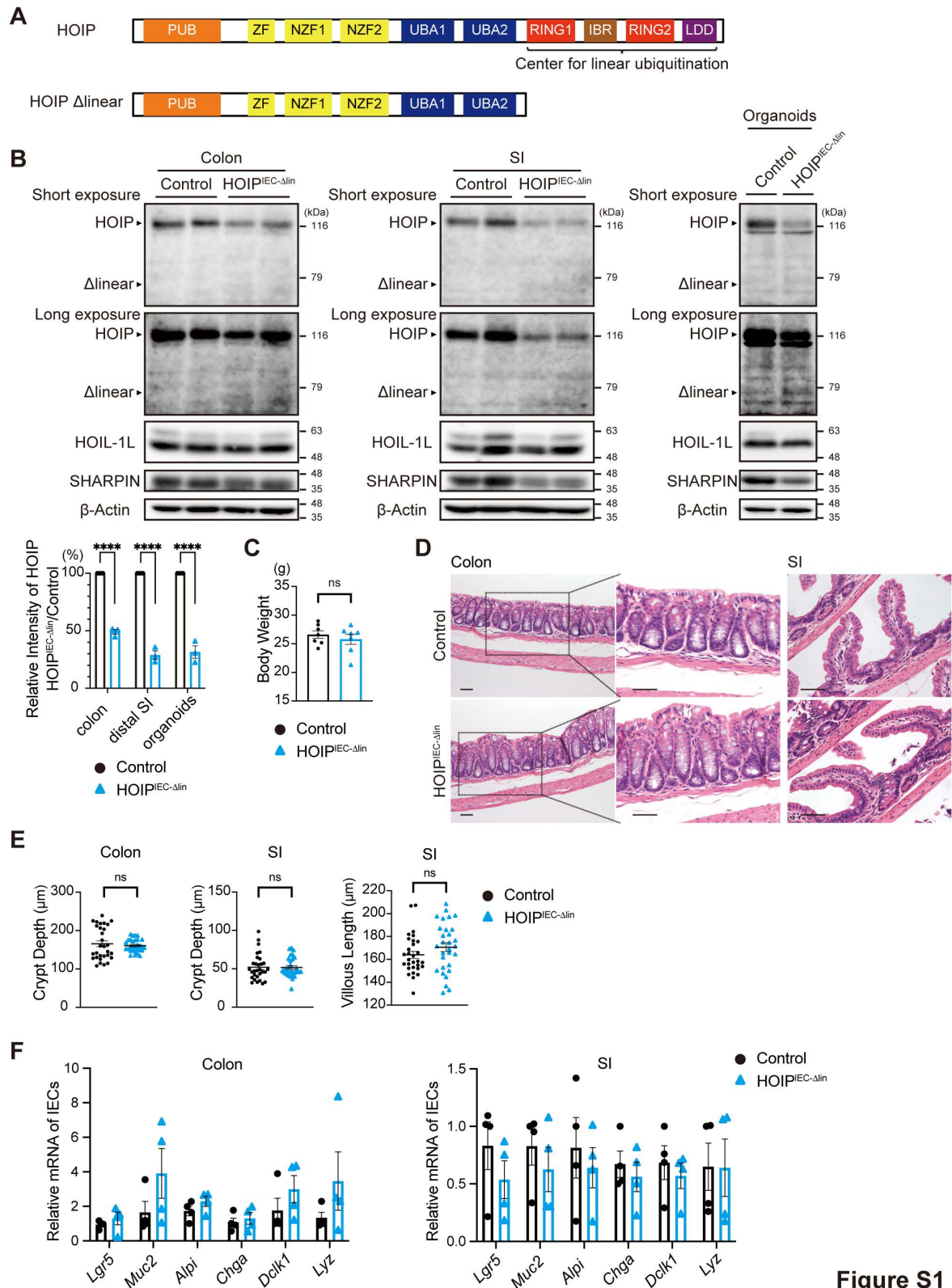
51 122 **ELISA**

52
53 123 Cell culture supernatants and serum were collected and stored at -80°C until use. The
54
55 124 concentrations of TNF, IL-6, and MCP-1/CCL2 in culture supernatants and serum were
56
57 125 measured using an ELISA MAX Standard Set (BioLegend). BD OPtEIA (BD Biosciences)
58
59
60

1
2
3 126 was used as the substrate. Absorbance at 450 nm, with a correction wave length of 570 nm,
4
5 127 was detected by a microplate reader (Molecular Devices, San Jose, CA, USA).
6
7
8 128

9
10 129 Flow cytometry
11

12 130 Primary cells isolated from the spleen or peripheral lymph nodes, or BMDMs, were incubated
13
14 131 with a mixture of the fluorochrome-conjugated antibodies. Samples were run on FACSCanto
15
16
17 132 II (BD Biosciences) using FACS Diva software v.6.1.2 (BD Biosciences). The results were
18
19
20 133 analyzed using FlowJo software v.9.9.6 (Tomy Digital Biology, Tokyo, Japan).
21
22 134

135 **Supplementary figures S1–S11****Figure S1**

136

137 **Figure S1. No morphological or developmental changes in the intestine of HOIP^{IEC-Δlin}**138 **mice under basal conditions.**

1
2
3 139 (A) Schematic illustration of the target region within the HOIP gene.
4
5 140 (B) Immunoblot analysis (top) of LUBAC subunits in lysates of IECs from the colon and the
6
7
8 141 small intestine (SI) and organoids of control and HOIP^{IEC-Δlin} mice. β-actin was used as a
9
10 142 loading control. Relative band intensity (bottom) of HOIP in HOIP^{IEC-Δlin} mice, normalized to
11
12 143 the intensity in littermate controls (n=3).
13
14
15 144 (C) Body weight of control and HOIP^{IEC-Δlin} mice under basal conditions (n=7). ns, not
16
17 145 significant.
18
19
20 146 (D) H&E staining of the colon and the small intestine from control and HOIP^{IEC-Δlin} mice
21
22 147 (n=3). Scale bars, 50 μm.
23
24
25 148 (E) Crypt length in the colon and small intestine, and villous length in the small intestine, of
26
27 149 control and HOIP^{IEC-Δlin} mice (n=30 fields per group).
28
29
30 150 (F) qRT-PCR analysis of expression of mRNA encoding epithelial markers by IECs from the
31
32 151 colon and small intestine of control and HOIP^{IEC-Δlin} mice (n=4). Data are normalized to
33
34 152 expression of *Gapdh* mRNA.
35
36 153 Statistical significance was determined by two-way ANOVA with Bonferroni's post-hoc test
37
38
39 154 (B, F) or a two-tailed unpaired Student's t test (C, E). ****P < 0.001.
40
41
42
43
44
45
46
47
48
49
50
51
52
53
54
55
56
57
58
59
60

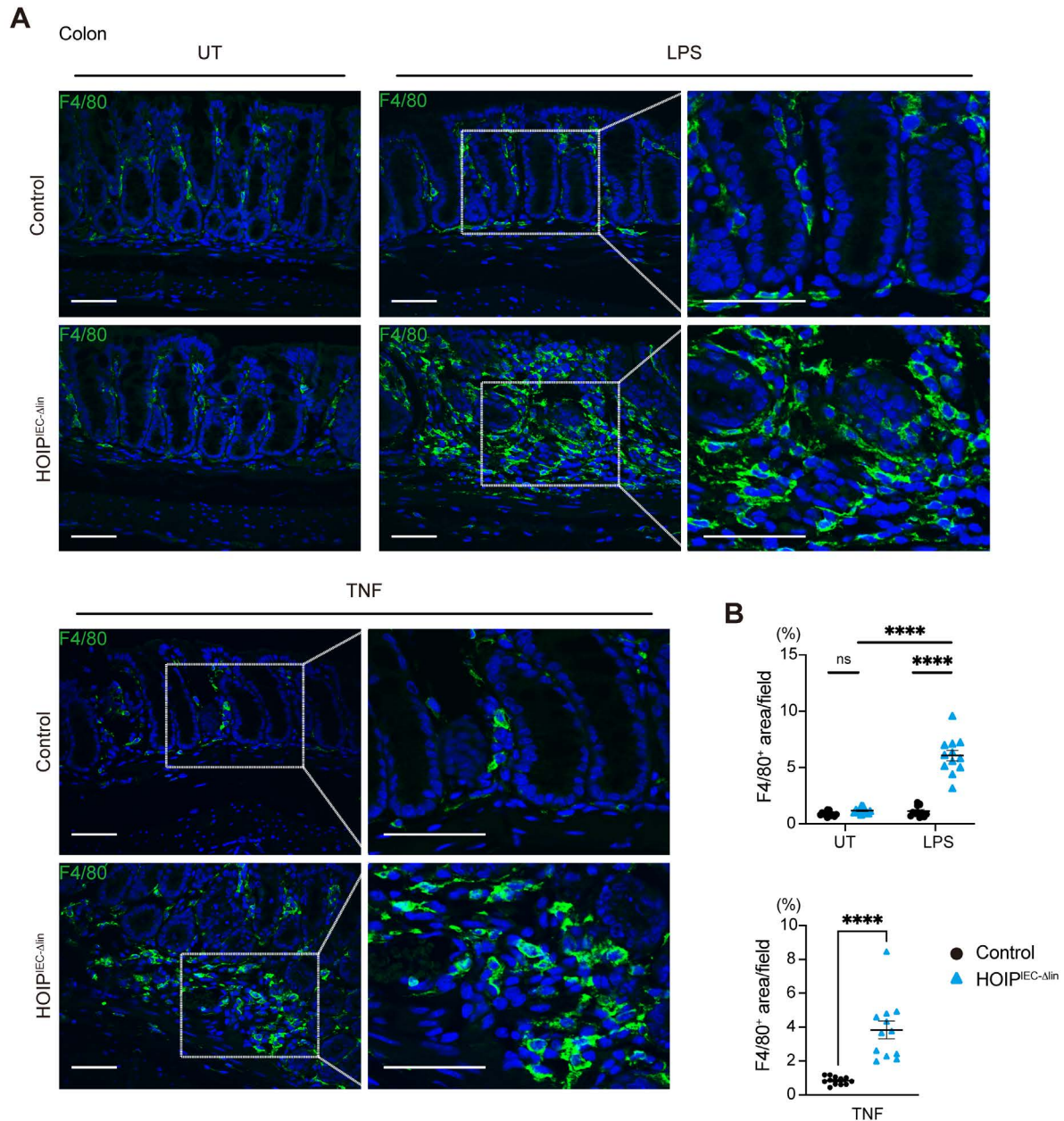


Figure S2

Figure S2. Immunofluorescence staining for F4/80 in distal colon sections from control and HOIP^{IEC-Δlin} mice after injection of LPS or TNF.

(A) Immunofluorescence staining for F4/80 in the distal colon 4 h post-injection of LPS or TNF (n=3). Data from untreated control (UT) and HOIP^{IEC-Δlin} mice are also shown (n=3).

Scale bars, 50 μm.

(B) Quantification of the F4/80⁺ cells in (A) (n=12 fields per group).

Statistical significance was determined by two-way ANOVA with Bonferroni's post-hoc

164 test (B, top), or a two-tailed unpaired Student's t test (B, bottom). **** $P < 0.001$.

165

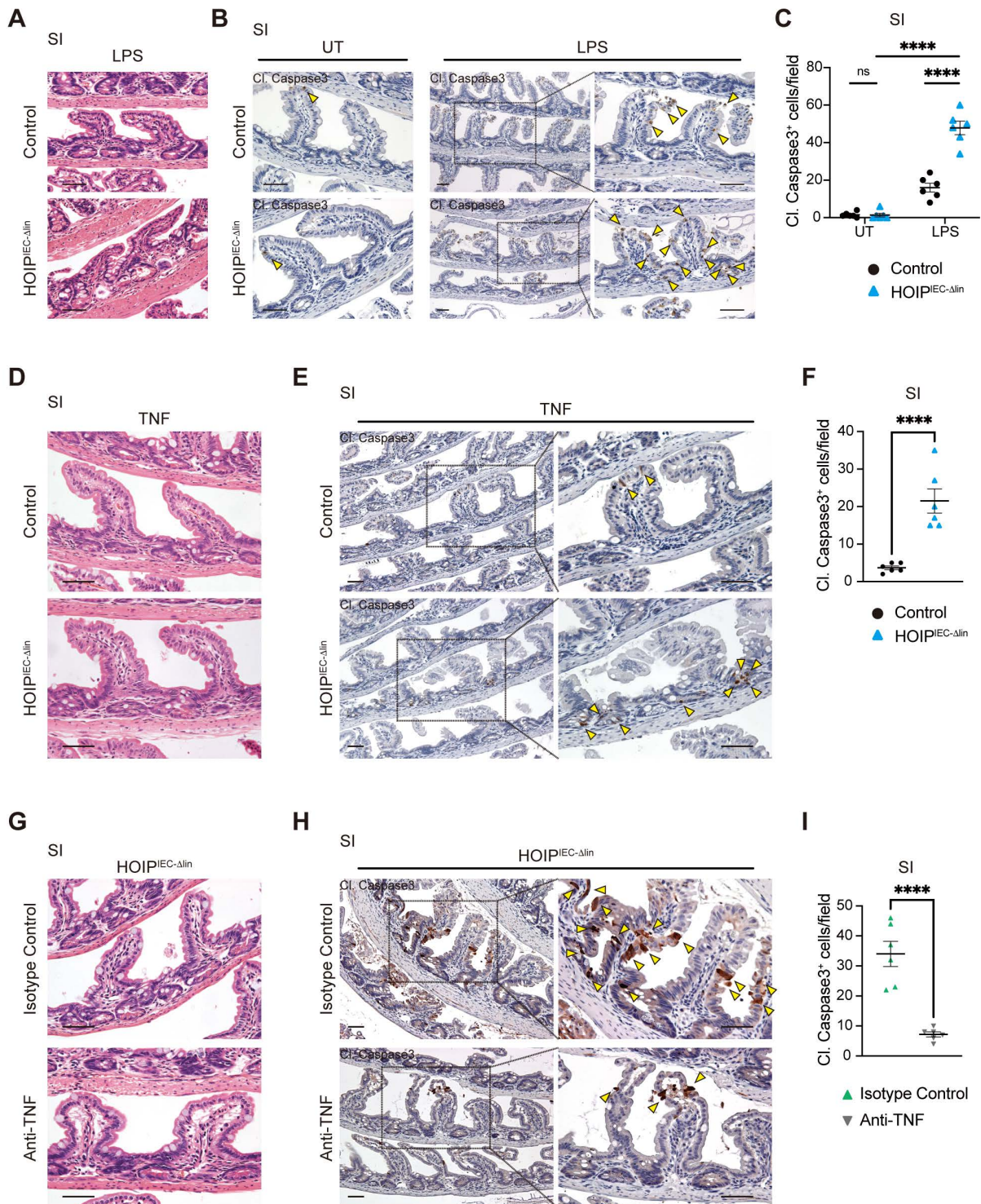


Figure S3

166

167 **Figure S3. TNF mediates IEC death in the small intestine of HOIP^{IEC-Δlin} mice upon LPS**
 168 **administration.**

1
2
3 169 (A) H&E staining of small intestine sections from control and HOIP^{IEC-Δlin} mice 24 h after
4
5
6 170 LPS administration (n=3). Scale bars, 50 μm.

7
8 171 (B) Immunohistochemical staining of cleaved caspase 3 (Cl. Caspase3) in sections of small
9
10 172 intestine at 1.5 h post-LPS treatment (n=3). Data of untreated control and HOIP^{IEC-Δlin} mice
11
12
13 173 are also shown (n=3). Yellow arrow heads show cells positive for cleaved caspase 3 in the
14
15 174 small intestine. Scale bars, 50 μm.

16
17
18 175 (C) Number of cleaved caspase 3-positive cells in the small intestine (n=6 fields per group).

19
20 176 (D) H&E staining of small intestine sections from control and HOIP^{IEC-Δlin} mice 24 h after
21
22 177 TNF treatment (n=3). Scale bars, 50 μm.

23
24
25 178 (E) Immunohistochemical staining of cleaved caspase 3 in the small intestine of control and
26
27 179 HOIP^{IEC-Δlin} mice 1.5 h post-TNF treatment (n=3). Yellow arrow heads show cells positive for
28
29 180 cleaved caspase 3. Scale bars, 50 μm.

30
31 181 (F) Number of cleaved caspase 3-positive cells in the small intestine (n=6 fields per group).

32
33
34 182 (G) H&E staining of the small intestine sections from isotype control- or anti-TNF-treated
35
36 183 HOIP^{IEC-Δlin} mice 24 h post-LPS administration (n=3). Scale bars, 50 μm.

37
38
39 184 (H) Immunohistochemical staining for cleaved caspase 3 in the small intestine of isotype
40
41 185 control- or anti-TNF-treated HOIP^{IEC-Δlin} mice 1.5 h post-LPS administration (n=3). Yellow
42
43 186 arrow heads show cells positive for cleaved caspase 3. Scale bars, 50 μm.

44
45
46 187 (I) Number of cleaved caspase 3-positive cells in the small intestine (n=6 fields per group).

47
48 188 Statistical significance was determined by two-way ANOVA with Bonferroni's post-hoc test

49
50 189 (C), or a two-tailed unpaired Student's t test (F, I). ****P < 0.001.

51
52
53 190

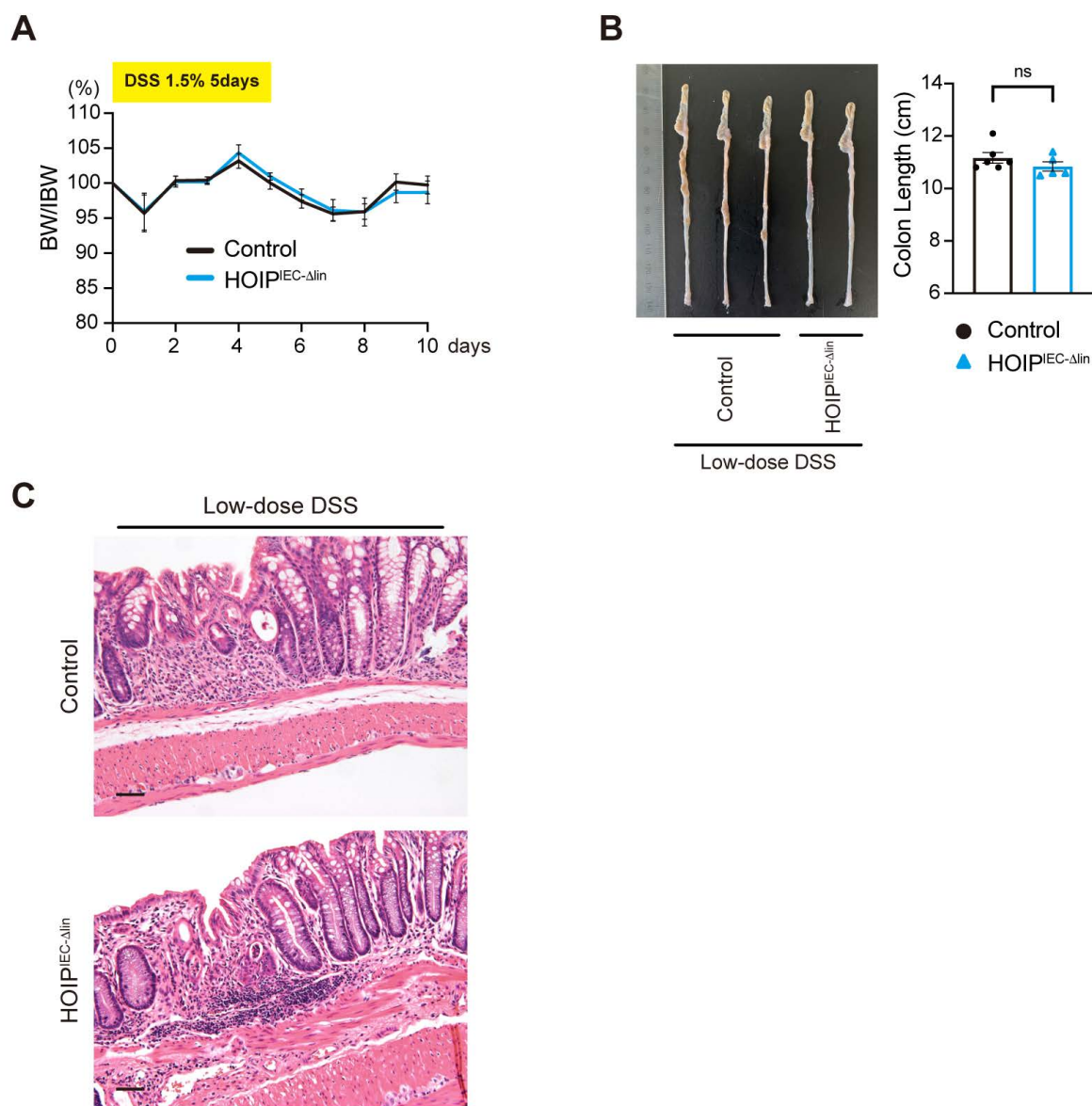


Figure S4

Figure S4. Loss of linear ubiquitination activity in IECs does not overtly affect the severity of low-dose DSS-induced colitis.

(A) Control and HOIP^{IEC-Δlin} mice were fed 1.5% DSS for 5 days. They were then fed regular water for 5 days. Body weight changes in control (n=6) and HOIP^{IEC-Δlin} mice (n=5) were measured during DSS treatment. BW, body weight; IBW, initial body weight.

(B) Representative pictures (left) and quantification of colon length (right) in DSS-treated control (n=6) and HOIP^{IEC-Δlin} mice (n=5).

(C) H&E staining of distal colon sections from control and HOIP^{IEC-Δlin} mice treated with

1
2
3
4
5
6
7
8
9
10
11
12
13
14
15
16
17
18
19
20
21
22
23
24
25
26
27
28
29
30
31
32
33
34
35
36
37
38
39
40
41
42
43
44
45
46
47
48
49
50
51
52
53
54
55
56
57
58
59
60

200 DSS (n=5). Scale bars, 50 μ m.

201 Statistical significance was determined by two-way ANOVA with Bonferroni's post-hoc test

202 (A), or by a two-tailed unpaired Student's t test (B).

203

For Peer Review

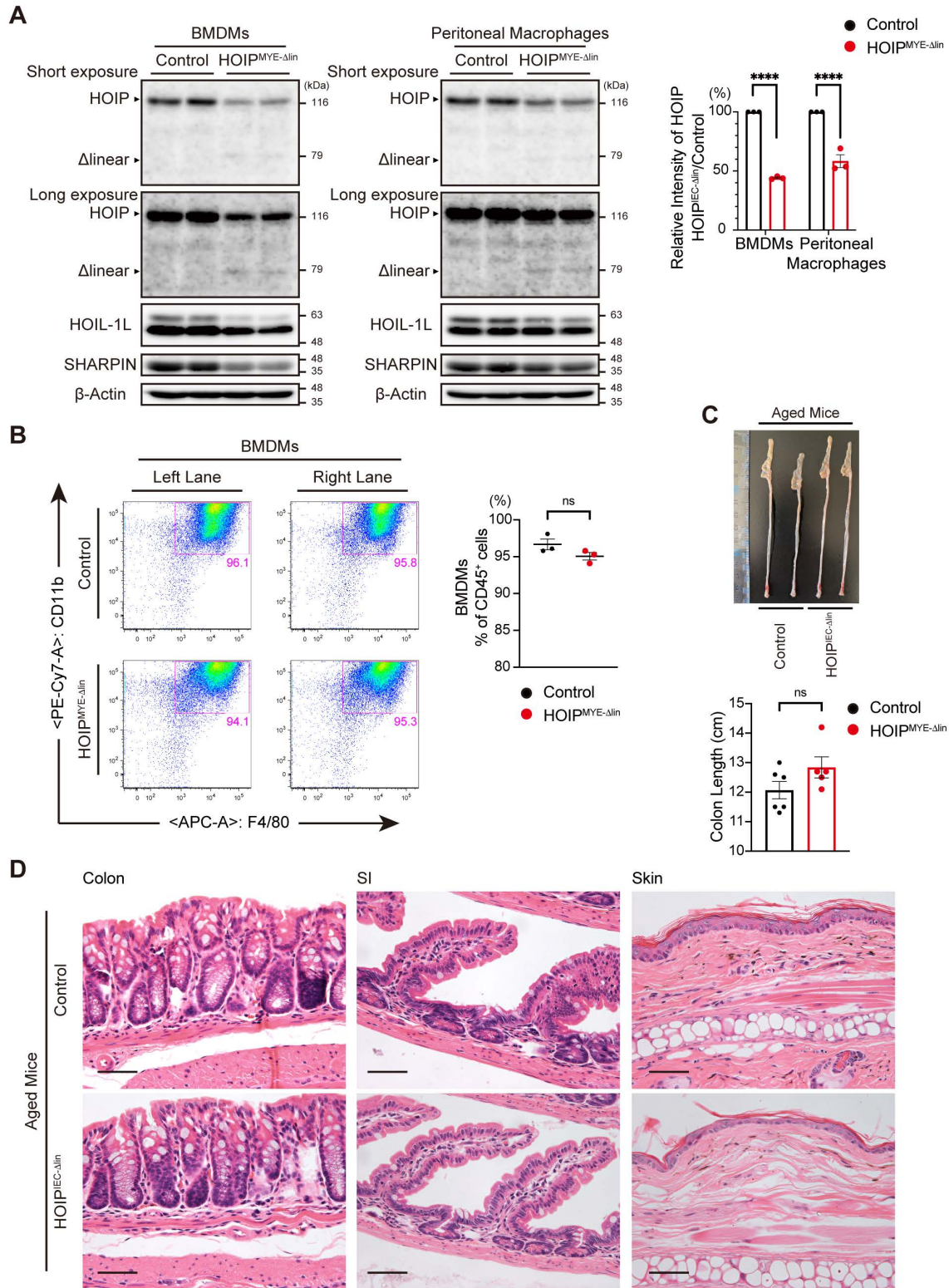


Figure S5

204
 205 **Figure S5. Aged HOIP^{MYE-Δlin} mice do not show inflammatory or autoimmune**
 206 **phenotypes under basal conditions.**

207 (A) Immunoblot analysis (left) of LUBAC subunits in lysates of BMDMs and peritoneal

1
2
3 208 macrophages from control and HOIP^{MYE-Δlin} mice. β-actin was used as a loading control.

4
5
6 209 Relative band intensity (right) of HOIP in HOIP^{IEC-Δlin} mice, normalized to the intensity in

7
8 210 littermate controls (n=3).

9
10 211 (B) Flow cytometry analysis of BMDM differentiation in (A) (left), and the proportion of
11
12 212 differentiated BMDMs (F4/80⁺CD11b⁺) among CD45⁺ cells (n=3) (right).

13
14
15 213 (C) Representative pictures (top), and quantification of colon length (bottom), from aged

16
17 214 control (n=6) and HOIP^{MYE-Δlin} mice (n=5). Aged mice were 24–32 weeks old.

18
19 215 (D) H&E staining of the colon, small intestine, and skin from aged control and HOIP^{MYE-Δlin}

20 216 mice (n=3). Scale bars, 50 μm.

21
22
23
24 217 Statistical significance was determined by two-way ANOVA with Bonferroni's post hoc-test

25
26 218 (A) or a two-tailed unpaired Student's t test (B, C). ****P < 0.001.

27
28
29 219

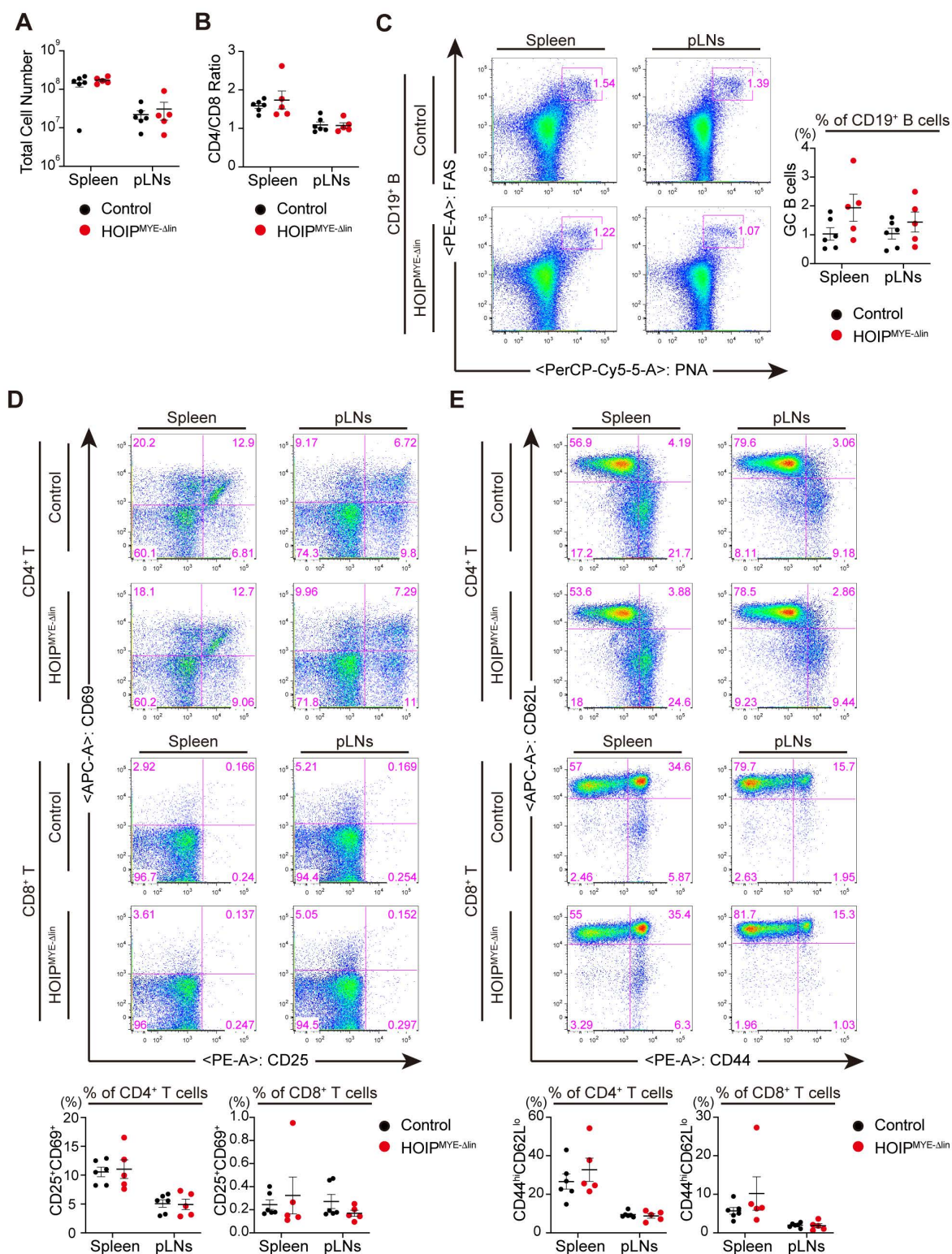


Figure S6

Figure S6. No overt changes in the proportion of activated lymphocytes in aged HOIP^{MYE-Δlin} mice under basal conditions.

(A) Total number of immune cells in the spleen and peripheral lymph nodes (pLNs) from

1
2
3 224 aged control (n=6) and HOIP^{MYE-Δlin} mice (n=5).
4

5 225 (B) Flow cytometry analysis of the CD4/CD8 T cell ratio in aged control (n=6) and
6
7
8 226 HOIP^{MYE-Δlin} mice (n=5).
9

10 227 (C) Representative flow cytometry plots (left) and percentages (right) of germinal center (GC)
11
12
13 228 B cells (PNA⁺FAS⁺) within the CD19⁺ B cell population in the spleen and pLNs of aged
14
15 229 control (n=6) and HOIP^{MYE-Δlin} mice (n=5).
16

17 230 (D) Representative flow cytometry plots (top) and percentages (bottom) of activated T cells
18
19
20 231 (CD25⁺CD69⁺) in the CD4⁺ and CD8⁺ T cell populations in the spleen and pLNs of aged
21
22 232 control (n=6) and HOIP^{MYE-Δlin} mice (n=5).
23

24 233 (E) Representative flow cytometry data (top) and percentages (bottom) of effector T cells
25
26
27 234 (CD44^{hi}CD62L^{lo}) in the CD4⁺ and CD8⁺ T cell populations in the spleen and pLNs of aged
28
29 235 control (n=6) and HOIP^{MYE-Δlin} mice (n=5).
30

31 236 Statistical significance was determined by two-way ANOVA with Bonferroni's post hoc-test
32
33
34 237 (A–E).
35

36 238
37
38
39
40
41
42
43
44
45
46
47
48
49
50
51
52
53
54
55
56
57
58
59
60

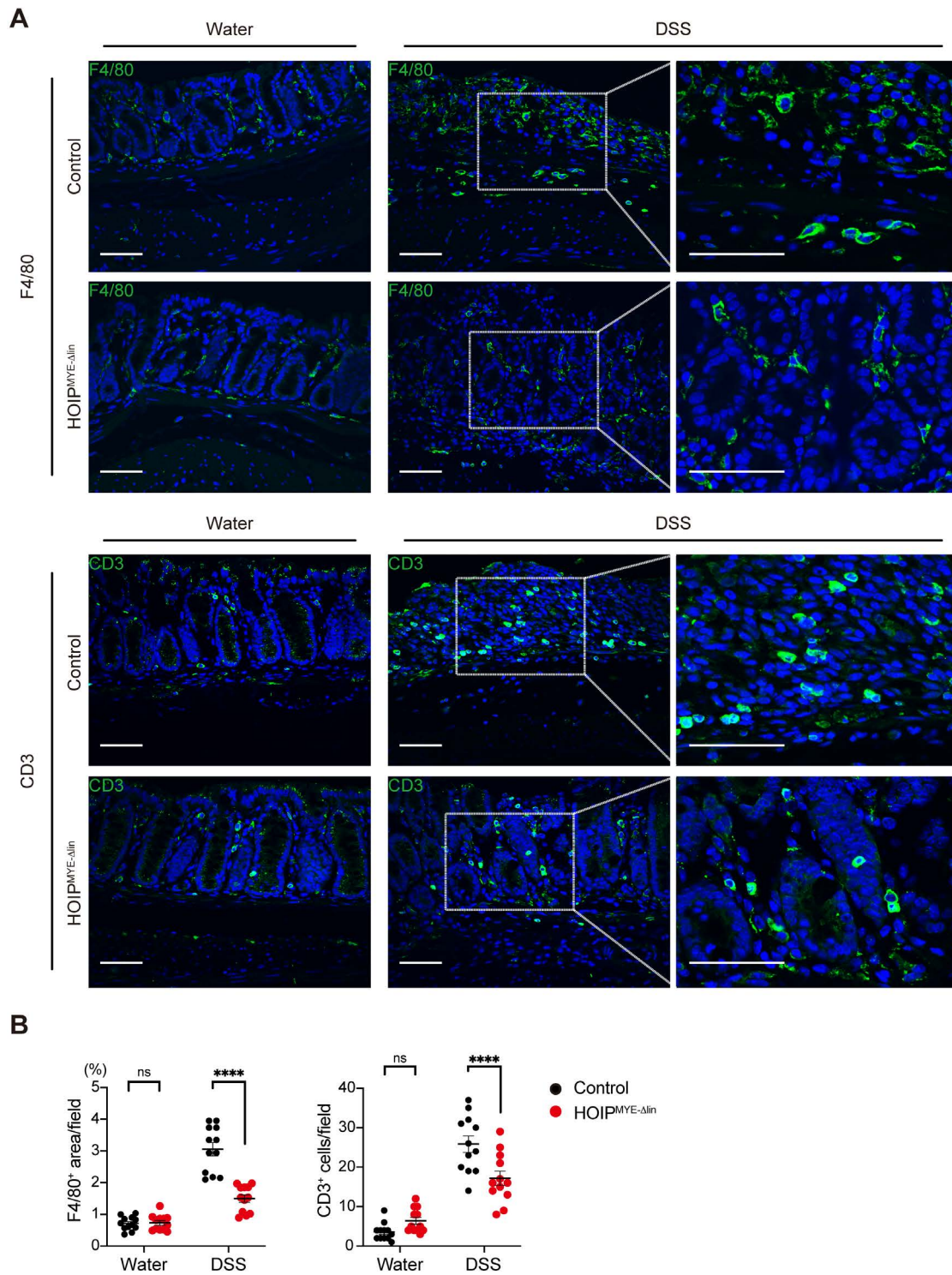


Figure S7

239

240 **Figure S7. Immunofluorescence staining of F4/80 and CD3 in distal colon sections from**
 241 **DSS-treated control and HOIP^{MYE-Δlin} mice.**

242 (A) Immunofluorescence staining for F4/80 and CD3 in distal colon sections from
 243 DSS-treated control and HOIP^{MYE-Δlin} mice (n=3). Data from untreated control and

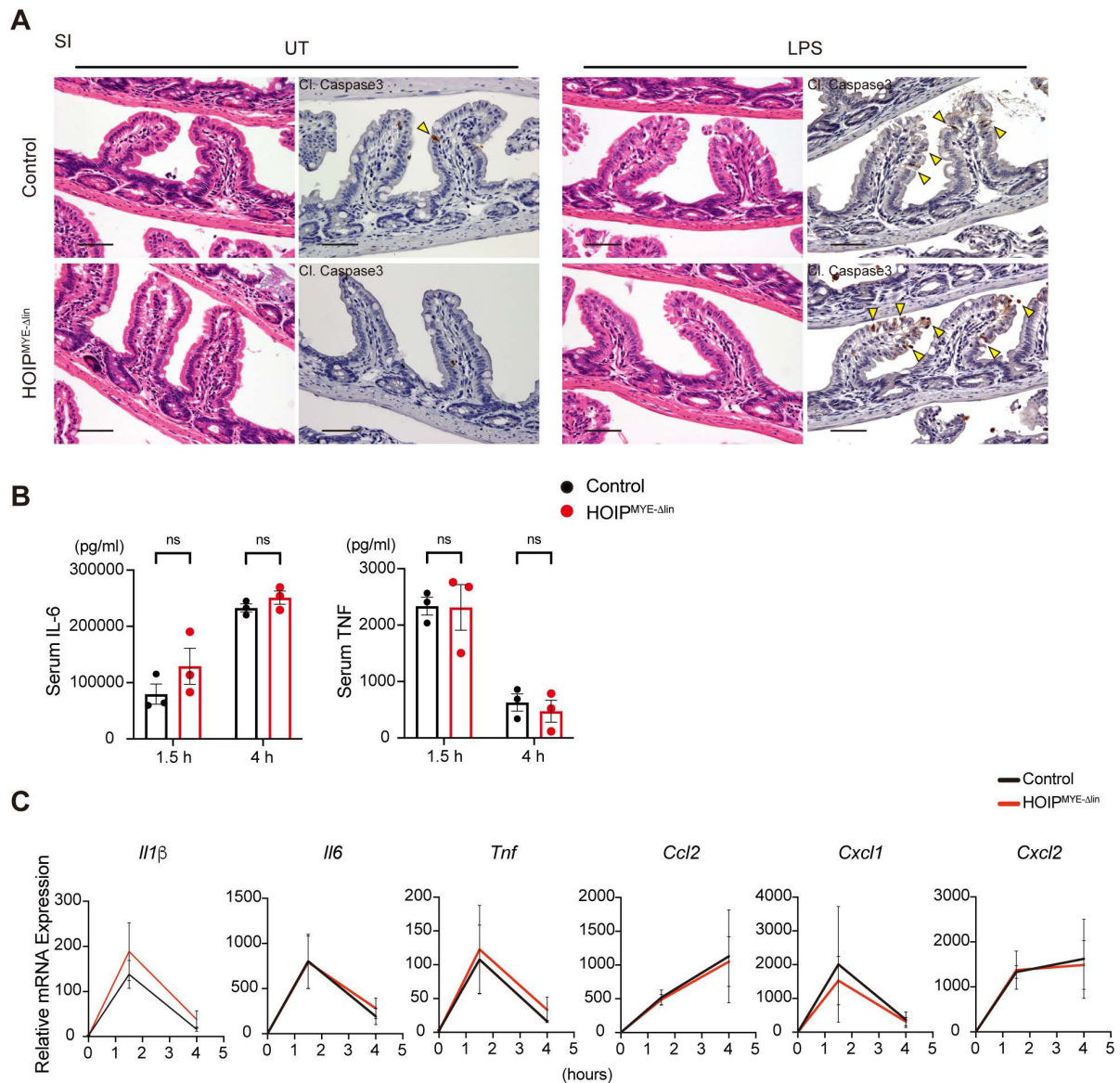
244 HOIP^{MYE-Δlin} mice are also shown (n=3). Scale bars, 50 μm.

245 (B) Quantification of immune cells in (A) (n=12 fields per group).

246 Statistical significance was determined by two-way ANOVA with Bonferroni's post hoc-test

247 (B).

248



249 **Figure S8**

250

251 **Figure S8. Attenuation of LUBAC ligase activity in macrophages has no effect in an**

252 **LPS-induced IEC shedding model.**

(A) H&E staining and immunohistochemical staining of small intestine sections for cleaved

1
2
3 253 caspase 3 at 1.5 h post-intraperitoneal administration of LPS to control and HOIP^{MYE-Δlin} mice
4
5
6 254 (n=3). Data from **untreated control** and HOIP^{MYE-Δlin} mice are also shown (n=3). Yellow
7
8 255 arrows head indicate cells positive for cleaved caspase 3. Scale bars, 50 μm.

9
10 256 **(B)** ELISA used to measure serum IL-6 and **TNF** levels in control and HOIP^{MYE-Δlin} mice after
11
12
13 257 LPS injection (n=3).

14
15 258 **(C)** qRT-PCR analysis of inflammatory cytokine and chemokine expression in colon tissue
16
17
18 259 from LPS-treated control and HOIP^{MYE-Δlin} mice (n=3). Data are normalized to expression of
19
20 260 *Gapdh* mRNA.

21
22 261 Statistical significance was determined by two-way ANOVA with Bonferroni's post-hoc test

23
24
25 262 **(B, C)**.

26
27 263

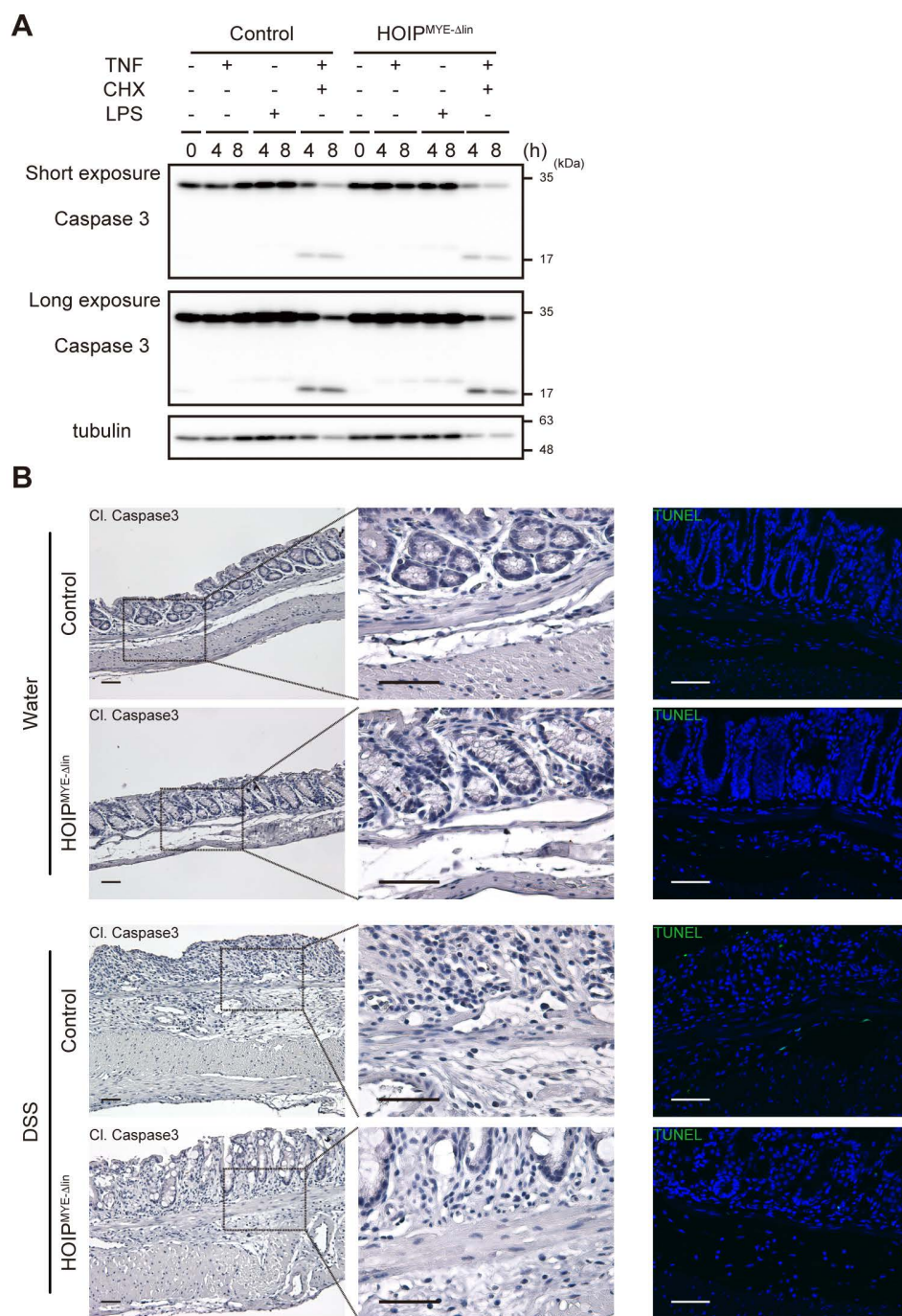


Figure S9

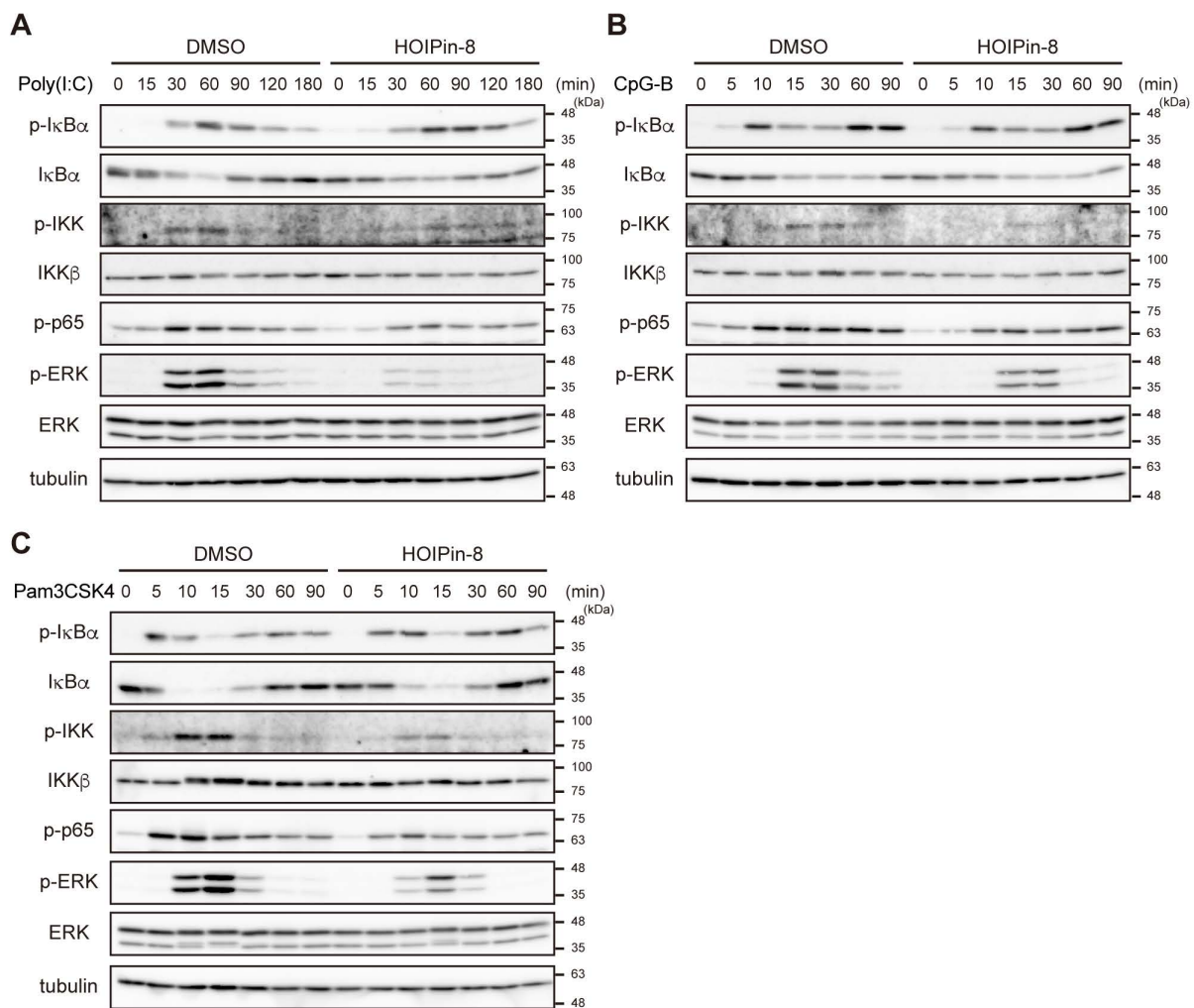
Figure S9. Impaired linear ubiquitination activity in macrophages has no overt effect on cell death.

(A) Immunoblot analysis of caspase 3 cleavage in BMDMs from control and HOIP^{MYE-Δlin} mice treated with TNF (10 ng/ml), LPS (10 ng/ml), or TNF (10 ng/ml) and CHX (20 μg/ml) for the indicated periods. Tubulin was used as a loading control. Data are representative of at

270 least two independent experiments.

271 (B) Immunohistochemical staining of the distal colon sections for cleaved caspase 3, and
 272 immunofluorescence TUNEL staining, in control and HOIP^{MYE-Δlin} mice treated with DSS
 273 (n=3). Data from untreated control and HOIP^{MYE-Δlin} mice are also shown (n=3). Scale bars,
 274 50 μm.

275



276 **Figure S10**

277 **Figure S10. Inhibiting LUBAC ligase activity impairs NF-κB and ERK activation upon**
 278 **stimulation by multiple TLR ligands.**

279 (A, B, C) BMDMs from WT mice were pre-treated for 30 min with DMSO or HOIPin-8 (10
 280 μM) and then stimulated with Poly(I:C) (2 μg/ml) (A), CpG-B (1 μM) (B), or Pam3CSK4 (1

281 $\mu\text{g/ml}$) (C) for the indicated times. Whole cell lysates were immunoblotted with the indicated
 282 antibodies. Tubulin was used as a loading control.
 283 A representative image of an immunoblot from at least two independent experiments is
 284 shown.

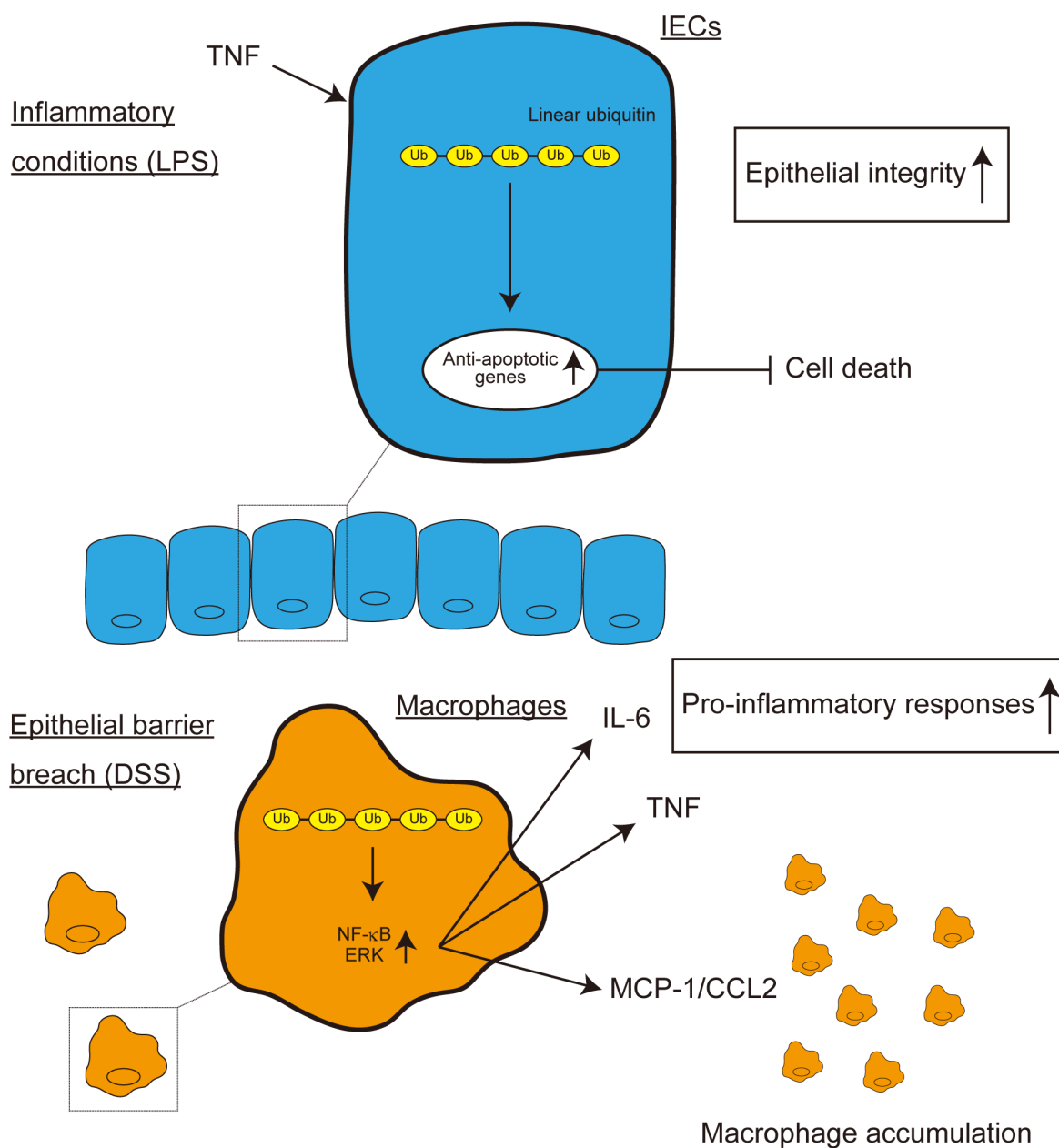


Figure S11

286
 287 **Figure S11. Schematic summarizing the different functions of linear ubiquitination in**

1
2
3 288 **IECs and macrophages.**
4

5 289 Under inflammatory conditions, linear ubiquitination in IECs regulates TNF-mediated
6
7 290 epithelial integrity by suppressing IEC death via up-regulation of anti-apoptotic genes. By
8
9 291 contrast, in the event of an epithelial barrier breach, linear ubiquitination in macrophages
10
11 292 regulates pro-inflammatory responses by producing pro-inflammatory cytokines (IL-6 and
12
13 293 TNF), and a chemokine that attracts macrophages (MCP-1/CCL2) downstream of activated
14
15
16
17 294 NF- κ B and ERK.
18
19

20 295
21
22
23
24
25
26
27
28
29
30
31
32
33
34
35
36
37
38
39
40
41
42
43
44
45
46
47
48
49
50
51
52
53
54
55
56
57
58
59
60

For Peer Review

1
2
3
4
5
6
7
8
9
10
11
12
13
14
15
16
17
18
19
20
21
22
23
24
25
26
27
28
29
30
31
32
33
34
35
36
37
38
39
40
41
42
43
44
45
46
47
48
49
50
51
52
53
54
55
56
57
58
59
60

296 **Supplementary table legends**

297 **Table S1. List of primers used for qPCR analysis**

For Peer Review

Table S1. List of primers used for qPCR analysis

Gene		Sequence
<i>Il1β</i>	Forward	5'-TGGACCTTCCAGGATGAGGACA-3'
	Reverse	5'-GTTTCATCTCGGAGCCTGTAGTG-3'
<i>Il6</i>	Forward	5'-TACCACTTCAACAAGTCGGAGGC-3'
	Reverse	5'-CTGCAAGTGCATCATCGTTGTTC-3'
<i>Tnf</i>	Forward	5'-GGTGCCTATGTCTCAGCCTCTT-3'
	Reverse	5'-GCCATAGAAGTATGAGAGGGAG-3'
<i>Ccl2</i>	Forward	5'-CCGGCTGGAGCATCCACGTGT-3'
	Reverse	5'-TGGGGTCAGCACAGACCTCTCTCT-3'
<i>Cxcl1</i>	Forward	5'-TCCAGAGCTTGAAGGTGTTGCC-3'
	Reverse	5'-AACCAAGGGAGCTTCAGGGTCA-3'
<i>Cxcl2</i>	Forward	5'-CCAACCACCAGGCTACAGG-3'
	Reverse	5'-GCGTCACACTCAAGCTCTG-3'
<i>Birc3</i>	Forward	5'-GGACATTAGGAGTCTTCCCACAG-3'
	Reverse	5'-GAACACGATGGATACCTCTCGG-3'
<i>Tnfaip3</i>	Forward	5'-AGCAAGTGCAGGAAAGCTGGCT -3'
	Reverse	5'-GCTTTCGCAGAGGCAGTAACAG -3'
<i>Nfkbia</i>	Forward	5'-GCCAGGAATTGCTGAGGCACTT-3'
	Reverse	5'-GTCTGCGTCAAGACTGCTACAC-3'
<i>Lgr5</i>	Forward	5'-CCTACTCGAAGACTTACCCAGT-3'
	Reverse	5'-GCATTGGGGTGAATGATAGCA-3'
<i>Muc2</i>	Forward	5'-GGTCCAGGGTCTGGA TCACA-3'
	Reverse	5'-GCTCAGCTCACTGCCA TCTG-3'
<i>Alpi</i>	Forward	5'-TCCTACACCTCCATTCTCTATGG-3'
	Reverse	5'-CCGCCTGCTGCTTGTAG-3'
<i>Chga</i>	Forward	5'-ATCCTCTCTATCCTGCGACAC-3'
	Reverse	5'-GGGCTCTGGTTCTCAAACACT-3'
<i>Dclk1</i>	Forward	5'-TACCGACGCTATCAAGCTGGAC-3'
	Reverse	5'-GGTAACGGAAGTCTCTGGTCC-3'
<i>Lyz</i>	Forward	5'-TGACATCACTGCAGCCATAC-3'
	Reverse	5'-TGGGACAGATCTCGGTTTTG-3'
<i>Gapdh</i>	Forward	5'-TTCACCACCATGGAGAAGGC-3'
	Reverse	5'-GGCATGGACTGTGGTCATGA-3'